Delft University of Technology

Long-eccentricity regulated climate control on fluvial incision and aggradation in the Palaeocene of north-eastern Montana (USA)

Noorbergen, Lars J.; Turtu, Antonio; Kuiper, Klaudia F.; Kasse, Cornelis ; van Ginneken, Sverre; Dekkers, Mark J.; Krijgsman, Wout; Abels, Hemmo A.; Hilgen, Frederik J.

Important note
To cite this publication, please use the final published version (if applicable).
Please check the document version above.

Long-eccentricity regulated climate control on fluvial incision and aggradation in the Palaeocene of north-eastern Montana (USA)

LARS J. NOORBERGEN* , ANTONIO TURTU*, KLAUDIA F. KUIPER*,
CORNELIS KASSE*, SVERRE VAN GINNEKEN†, MARK J. DEKKERS†,
WOUT KRIJGSMAN†, HEMMO A. ABELS‡ and FREDERIK J. HILGEN†
*Department of Earth Sciences, VU University Amsterdam, De Boelelaan 1085, Amsterdam 1081 HV,
The Netherlands (E-mail: l.j.noorbergen@gmail.com)
†Department of Earth Sciences, Utrecht University, Princetonlaan 8a, Utrecht 3584 CB, The
Netherlands
‡Department of Geosciences and Engineering, Delft University of Technology, Stevinweg 1, Delft 2628
CN, The Netherlands

ABSTRACT

Aggradation and fluvial incision controlled by downstream base-level changes at timescales of 10 to 500 kyr is incorporated in classic sequence stratigraphic models. However, upstream climate control on sediment supply and discharge variability causes fluvial incision and aggradation as well. Orbital forcing often regulates climate change at 10 to 500 kyr timescales while tectonic processes such as flexural (un)loading exert a dominant control at timescales longer than 500 kyr. It remains challenging to attribute fluvial incision and aggradation to upstream or downstream processes or disentangle allogenic from autogenic forcing, because time control is mostly limited in fluvial successions. The Palaeocene outcrops of the fluvial Lebo Shale Member in north-eastern Montana (Williston Basin, USA) constitute an exception. This study uses a distinctive tephra layer and two geomagnetic polarity reversals to create a 15 km long chronostratigraphic framework based on the correlation of twelve sections. Three aggradation–incision sequences are identified with durations of approximately 400 kyr, suggesting a relation with long-eccentricity. This age control further reveals that incision occurred during the approach of – or during – a 405 kyr long-eccentricity minimum. A long-term relaxation of the hydrological cycle related to such an orbital phasing potentially exerts an upstream climate control on river incision. Upstream, an expanding vegetation cover is expected because of an increasingly constant moisture supply to source areas. Entrapping by vegetation led to a significantly reduced sediment supply relative to discharge, especially at times of low evapotranspiration. Hence, high discharges resulted in incision. This study assesses the long-eccentricity regulated climate control on fluvial aggradation and incision in a new aggradation–incision sequence model.

Keywords Aggradation, climate change, fluvial stratigraphy, hiatuses, incision, long-eccentricity cycle, magnetostratigraphic correlation, tephrostratigraphic correlation.

INTRODUCTION

Many fluvial successions are built by aggradation intermittently interrupted by degradation (incision), operating at 10 kyr to 10 Myr timescales. Aggradation occurs when sediment supply is significantly higher than maximum bedload transport rate, and incision occurs when sediment supply is significantly lower than bedload transport rate. Both aggradation and incision are controlled by internal (autogenic) and/or external (allogenic) factors on sediment supply (Mackin, 1948; Leopold & Bull, 1979; Blum & Törnqvist, 2000; Catuneanu, 2006; Holbrook *et al.*, 2006; Miall, 2014). On 10 kyr to 10 Myr timescales, fluvial incision and aggradation are attributed to an interplay of allogenic controls: geomorphic base-level (i.e. sea-level, lake-level, or a drainage network trunk channel axis), climate and tectonics (e.g. Schumm, 1993; Shanley & McCabe, 1994; Ethridge *et al.*, 1998; Miall, 2014). Base-level change remains a major cause for fluvial incision and aggradation in sequence stratigraphic models (e.g. Posamentier & Vail, 1988; Wright & Marriott, 1993; Shanley & McCabe, 1994). Accordingly, base-level fall causes incision and base-level rise causes aggradation. Nevertheless, the sequence stratigraphic model cannot simply be applied to every fluvial setting. If, and how, base-level change causes aggradation or incision depends in particular on the difference between the coastal plain and shelf gradient, the river's ability to self-accommodate by adapting channel sinuosity, and the landward limit of base-level influence (Schumm, 1993; Blum & Törnqvist, 2000). Base-level change may be controlled downstream by eustasy and upstream by sediment supply. Greenhouse worlds feature only minor or no polar ice-caps which makes glacio-eustasy as a mechanism for base-level control unlikely. In contrast, aquifer-eustasy (i.e. the imbalance in continental water storage in lakes and groundwater and continental water release to the ocean) driven by eccentricity-forced climate changes may control higher-order global sea-level fluctuations of *ca* 30 m (Sames *et al.*, 2016; Wendler & Wendler, 2016; Wendler *et al.*, 2016). In addition to downstream control by aquifer-eustasy, orbital-forced climate changes in the hinterland (i.e. precipitation, weathering and vegetation), that influence sediment supply and discharge, exert an important upstream control on sedimentation at the basin-scale (Fielding &

Webb, 1996; Abels *et al.*, 2013; Noorbergen *et al.*, 2018).

Orbital control is difficult to separate from time-overlapping tectonic forcing (e.g. Holbrook & Schumm, 1999) and autogenic processes (e.g. Hajek & Straub, 2017). This is mainly due to poor age control in pre-Quaternary archives (Blum & Törnqvist, 2000; Abels *et al.*, 2013). It precludes proper assessment of timescales, lateral extents of facies and inter-facies connections. Not surprisingly, only a few pre-Quaternary studies have documented impacts of orbital-forced climate changes on sedimentation in fluvial systems (Olsen, 1990; Olsen *et al.*, 1994; Fielding & Webb, 1996; Abels *et al.*, 2013; Noorbergen *et al.*, 2018). These studies deal with fluvial stratigraphic architectures that are dominated by aggradation and lack valley-related unconformable surfaces. It thus remains unknown how orbital-forced climate change may influence aggradation and incision in pre-Quaternary greenhouse fluvial systems.

The Palaeocene Lebo Shale Member of the Fort Union Formation, Williston Basin (north-eastern Montana, USA), provides the rare opportunity to investigate the control mechanisms related to fluvial aggradation and incision under greenhouse climate conditions and at the timescales of interest. For this purpose, a *ca* 15 km long north–south oriented stratigraphic fence panel, based on detailed stratigraphic logging of parallel sections in combination with magnetostratigraphic and tephrostratigraphic correlations and tracing of stratigraphic marker levels, such as coals and palaeosols, has been generated in McCone County (north-eastern Montana, USA).

GEOLOGICAL SETTING

The lower Fort Union Formation in the Williston Basin

During Cretaceous time, the intracratonic Williston Basin was encapsulated in the Western Interior Foreland Basin (DeCelles, 2004). Depositional environments in the Williston Basin were mainly marine in the mid-Cretaceous but these became replaced by the alluvial systems of the Laramide orogeny taking place from the late Cretaceous into the Eocene (Cherven & Jacob, 1985). Approximately half-way through the Laramide uplift, in the early Palaeocene, fluvio-deltaic sediments of

the Fort Union Formation were deposited. In the Williston Basin, the lower Palaeocene part of the Fort Union Formation is exposed in the badlands of the Missouri River and its tributaries, broadly covering the region between eastern-Montana and central-Dakota (Fig. 1A). The base of the Fort Union Formation is represented by the first laterally extensive coal seams at – or close to – the K-Pg boundary (Fastovsky & Bercovici, 2016). The top of the lower Fort Union Formation, at the base of the Tongue River Member, is represented by a few metres thick bleached palaeo-weathering zone (i.e. the Rhame Bed) that might represent a hiatus of a few million years of middle Palaeocene time (Warwick *et al.*, 2004). The lower Fort Union Formation has been subdivided into five members that are partly lateral equivalents; the Tullock, Lebo Shale, Ludlow, Slope and Cannonball members (stratigraphic relations, Fig. 1B).

The Lebo Shale Member

The Lebo Shale Member (Stone & Calvert, 1910) consists of greyish-yellow sand-dominated intervals and grey mud-dominated intervals, both containing several coal seams and bleached zones (Collier & Knechtel, 1939; Rigby & Rigby, 1990). The sand-dominated intervals are laterally extensive and form erosion-resistant caps on top of buttes and ridges. These have been interpreted as channel-splay systems (Rigby & Rigby, 1990) with point-bar deposition along meandering streams (Diemer & Belt, 1991). The mud-dominated intervals contain coaly organic material and locally contain lenses of coal and carbonaceous shale. If enriched in shale, these units typically show a sombre and bentonitic (as 'dirty-popcorn') surface weathering (Rigby & Rigby, 1990). They have been deposited in moderately saline playas with low carbonate concentrations (Rigby & Rigby, 1990). The coals are sub-bituminous to lignite in rank (Collier & Knechtel, 1939; Rigby & Rigby, 1990) and contain abundant vitrain alternated by dull-black powdery material (Rigby & Rigby, 1990). Coals in the Lebo Shale Member may have been formed in raised mires (Flores & Keighin, 1999; Flores *et al.*, 1999). Bleached zones are whitish laterally extensive markers and have been interpreted as the leaching-horizons of palaeosols (Rigby & Rigby, 1990).

The presence of dark-grey shales is the lithological criterion to distinguish the Lebo Shale Member from the underlying grey–gold–brownish thinly banded siltstones of the Tullock Member (e.g. Rigby & Rigby, 1990). Accordingly, the contact between the two members is placed at the base of the first distinct dark-grey shales just above the W-coal zone (Noorbergen *et al.*, 2018). In McCone County, distinct coal beds in the Fort Union Formation have been locally traced and regionally mapped based on topographic extrapolations (Collier & Knechtel, 1939). Collier & Knechtel (1939) assigned these coal beds reverse alphabetic labels, from 'Z' to 'P'. Given the Tullock–Lebo Shale lithostratigraphic contact as defined in Noorbergen *et al.* (2018), the Lebo Shale Member in McCone County includes coal beds 'V', 'U' and 'T' of Collier & Knechtel (1939). In the study area (Fig. 1D) only bed U has been mapped by Collier & Knechtel (1939). Because each coal bed of Collier & Knechtel (1939) is generally part of a larger cluster consisting of multiple coals, they are referred to as 'zones' in this work. Within the coal zones, individual coal beds can be up to 2 m thick but still contain centimetre-scale detrital partings and centimetre to decimetre-scale intervals with volcanic ash or sharp millimetre to centimetre-scale ash intercalations (i.e. tephras). The tephras contain euhedral crystals which enables their distinction from detrital partings that contain rounded minerals as the result of abrasion. Because of its abundant tephras (more than 20) and detrital partings, Collier & Knechtel (1939) held the U-coal zone, as being identical to the Big Dirty coal zone. In this matter, these authors followed the definition of Woolsey *et al.* (1917) of a high ash content coal zone in the Bull Mountain coal field, at a distance of *ca* 300 km south-west of McCone County.

METHODS

Sections and palaeo-flow measurements

In McCone County, 12 sections have been logged in four isolated outcrop areas that are from north to south: Coal Mine Divide (CMD); Rough Prong (RP); Radiotower (RT); and Horse Creek Road (HCR). There are at least two sections in each outcrop area; a central main section (the last character is 'M', for example CMD-M) and one or more other sections at a maximum distance of *ca* 3 km from the main section (the last character is the compass direction with respect to main section, for example CMD-W is west of the main section at Coal Mine Divide).
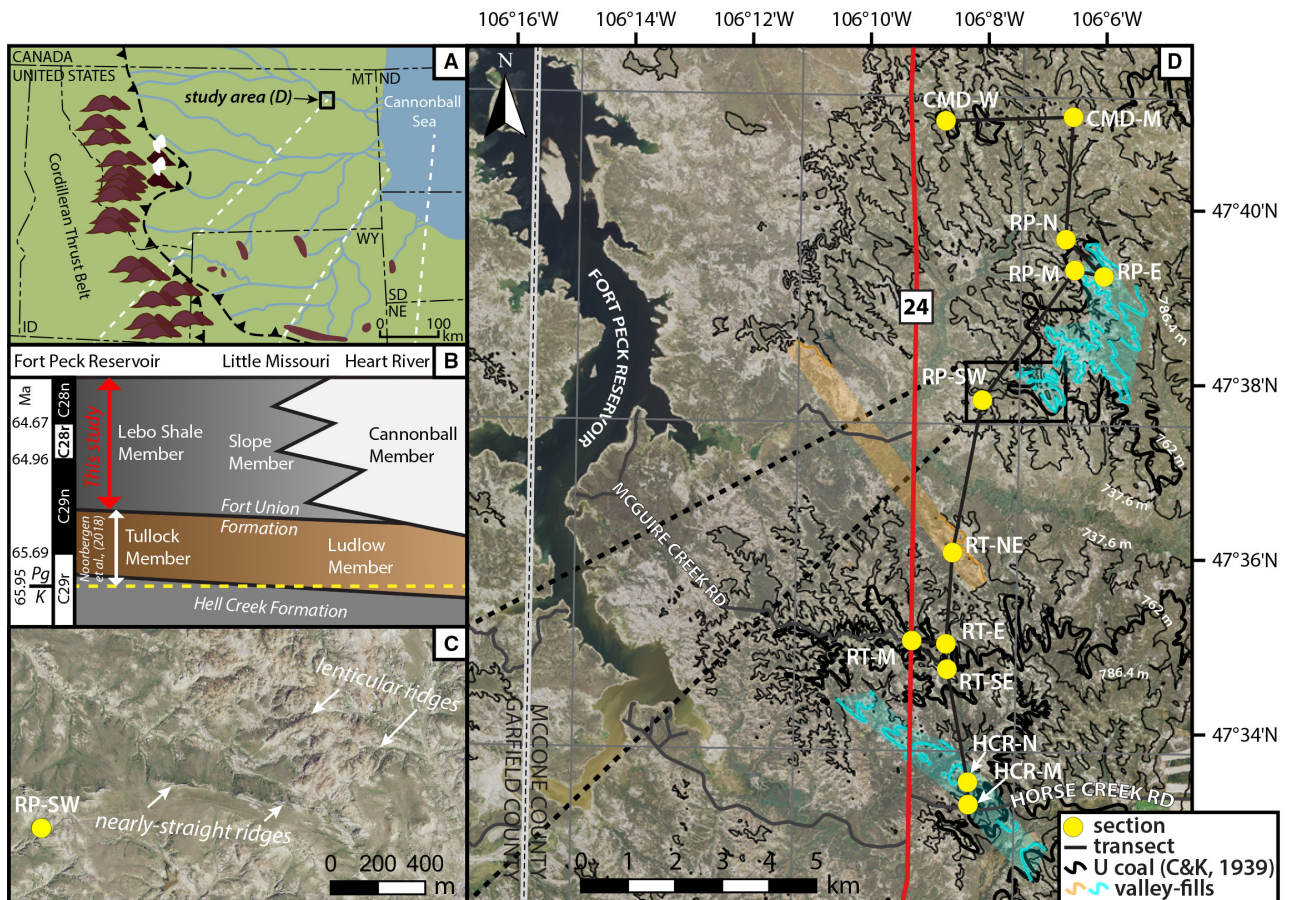
Fig. 1. Geographic and geological setting of the study area in McCone County, north-eastern Montana (USA). (A) Environmental reconstruction of Montana and adjacent states (modified from Flores, 2003). Peat mires were dissected by low sediment load rivers that drained into the Cannonball Sea in the early Palaeocene, approximately 65 Ma. Dashed white lines show map locations projected on the lithostratigraphic diagram of panel (B). (B) Along-profile cross-sectional diagram of lithostratigraphic units comprising Chron C29r to Chron C28n (modified from Johnson *et al.*, 2002). Study interval of Lebo Shale Member in north-eastern Montana is indicated (red arrow), stratigraphically above the Tullock Member studied by Noorbergen *et al.* (2018; white arrow). (C) Enlarged area from (D). Figure shows lenticular ridges belonging to the muddy point-bar deposits of Facies B1 (Table 1). (D) Ortho-image of the study area with 24.4 m (80 feet) elevation contour lines. Facies B1 valley-fill deposits are coloured orange for aggradation–incision sequence 1 (AIS-1) and cyan for AIS-2. Thick black solid line shows field mapping of coal bed U by Collier & Knechtel (1939). The locations of the sections (yellow circles) are connected by a solid black line showing the transect of the fence panel (Fig. 7). Section abbreviations (from north to south): CMD-W = Coal Mine Divide West; CMD-M = Coal Mine Divide Main; RP-N = Rough Prong North; RP-E = Rough Prong East; RP-M = Rough Prong Main; RP-SW = Rough Prong Southwest; RT-NE = Radiotower Northeast; RT-E = Radiotower East; RT-M = Radiotower Main; RT-SE = Radiotower Southeast; HCR-N = Horse Creek Road North; HCR-M = Horse Creek Road Main. Orthoimagery, quadrangle and road data were obtained from the Montana Spatial Data Infrastructure (MSDI) (http://geoinfo.msl.mt.gov/Home/msdi).

Palaeo-flow directions were measured from the dip planes of different sets of decimetre-scale cross-bedded sandstone that were interpreted as mid-channel bars. Channel axis orientations were determined perpendicular to the dip plane of lateral accretion planes that were interpreted as point-bars. Both sources of palaeo-flow data were plotted onto separate rose diagrams. No corrections for tectonic dip were required because the layers of the Fort Union Formation in north eastern Montana are dipping less than 1°.

Palaeomagnetism

All samples for palaeomagnetic analysis were taken in trenches, from unweathered rock at

least 1 m below the surface. A total of 243 levels were sampled within eight sections with an average sampling resolution of 0.5 m. Standard core samples (diameter = 2.54 cm) were taken with an electric, battery-powered drill using water as a coolant and oriented with a Brunton compass fixed to a Pomeroy orientation shaft (Brunton Inc., Riverton, Wyoming, USA). For each level it was attempted to drill multiple cores or one core of sufficient length so that the sample could be split into at least two specimens, enabling both thermal (TH) and alternating field (AF) demagnetization.

Previous rock magnetic analyses in the lower Fort Union Formation showed that the dominant magnetic remanence carriers are magnetite and maghemite (Swisher *et al.*, 1993; Sprain *et al.*, 2016). Intermediate-composition titanohematite could also be present and, if abundant, this mineral might complicate palaeomagnetic interpretations because of its ability to self-reverse (Sprain *et al.*, 2016). Previous magnetostratigraphic results of the lower Fort Union Formation in this area (Swisher *et al.*, 1993; LeCain *et al.*, 2014; Noorbergen *et al.*, 2018; Sprain *et al.*, 2018) are mutually consistent and in line with the Geomagnetic Polarity Timescale (Ogg, 2012). Therefore, self-reversal of intermediate titanohematite is a minor issue. In this study, TH demagnetization was done on 219 samples and AF demagnetization on 205. Of the total of 243 sampling horizons, 172 could be processed with both TH and AF demagnetization. More detailed procedures for the TH and AF demagnetization experiments are described in Noorbergen *et al.* (2018).

Inclination and declination components of the Characteristic Remanent Magnetization (ChRM) were determined using the REMASOFT 3.2 software program (Chadima & Hrouda, 2006). Plots were exported from Paleomagnetism.org (Koymans *et al.*, 2016). The ChRM directions were determined by anchored principal component analysis (PCA) (Kirschvink, 1980) if the sample clearly trended towards the origin along at least four consecutive demagnetization levels. If a sample showed no clear trend towards the origin, but a clustering of higher coercivity vector end-points, Fisher statistics (Fisher, 1953) were used to calculate the mean direction of that cluster. Data points with a mean angular deviation (MAD) <15° of the anchored fit or a MAD <15° of the Fisher mean (note: The MAD in Remasoft shown for the Fisher mean is the alpha95 of the Fisher mean) are connected

(Fig. 2). Samples with a ChRM, but with a MAD >15°, are displayed with open symbols. The data were not corrected for the present-day local declination in the study area of 9.3° (Thébault *et al.*, 2015), because for the purpose of this paper (determining whether polarity was normal or reversed) the data are conclusive.

Scaling, vertical optimization and correlation of sections

From north (left) to south (right), along the transect (Fig. 1), stratigraphic logs of the sections were plotted on a 1 : 80 000 horizontal scale and a 1 : 600 vertical scale (Fig. 7). Two geomagnetic polarity reversals and one distinctive tephra ('the Sugar Ash') were used to optimize their vertical positions with respect to a backbone section (Coal Mine Divide West, CMD-W) in which all three chronostratigraphic markers are present. For the polarity reversals the midpoint of the reversal interval was used as absolute value (Figs 3 and 8). From the five sections that contained all three markers, CMD-W was selected as backbone, because the stratigraphic spacing of the markers in this section best represented the entire study area. The position of polarity reversals in sections lacking palaeomagnetic data was estimated by correlating the Sugar Ash and/or field tracing coal seams to nearby sections (at <3 km distance) that recorded the reversal to increase the number of optimization tie-points. Prediction of polarity reversals include the lower reversal in Rough Prong North (RP-N), Rough Prong Main (RP-M) and Radiotower Northeast (RT-NE), and both the lower and upper reversals in Rough Prong Southwest (RP-SW), Radiotower East (RT-E) and Horse Creek Road North (HCR-N). For the vertical optimization, the same approach was used as in Noorbergen *et al.* (2018). After scaling and vertical optimization, sections were correlated, using the three chronostratigraphic markers. On the basis of this chronostratigraphic fence panel, the stratigraphic architecture of the three facies associations (Table 1) was interpreted.

RESULTS

Magnetostratigraphy

The polarities can be divided into four groups: (i) reversed polarity (24.3%); (ii) normal polarity (56.1%); (iii) uncertain polarity (14.6%); and (iv)
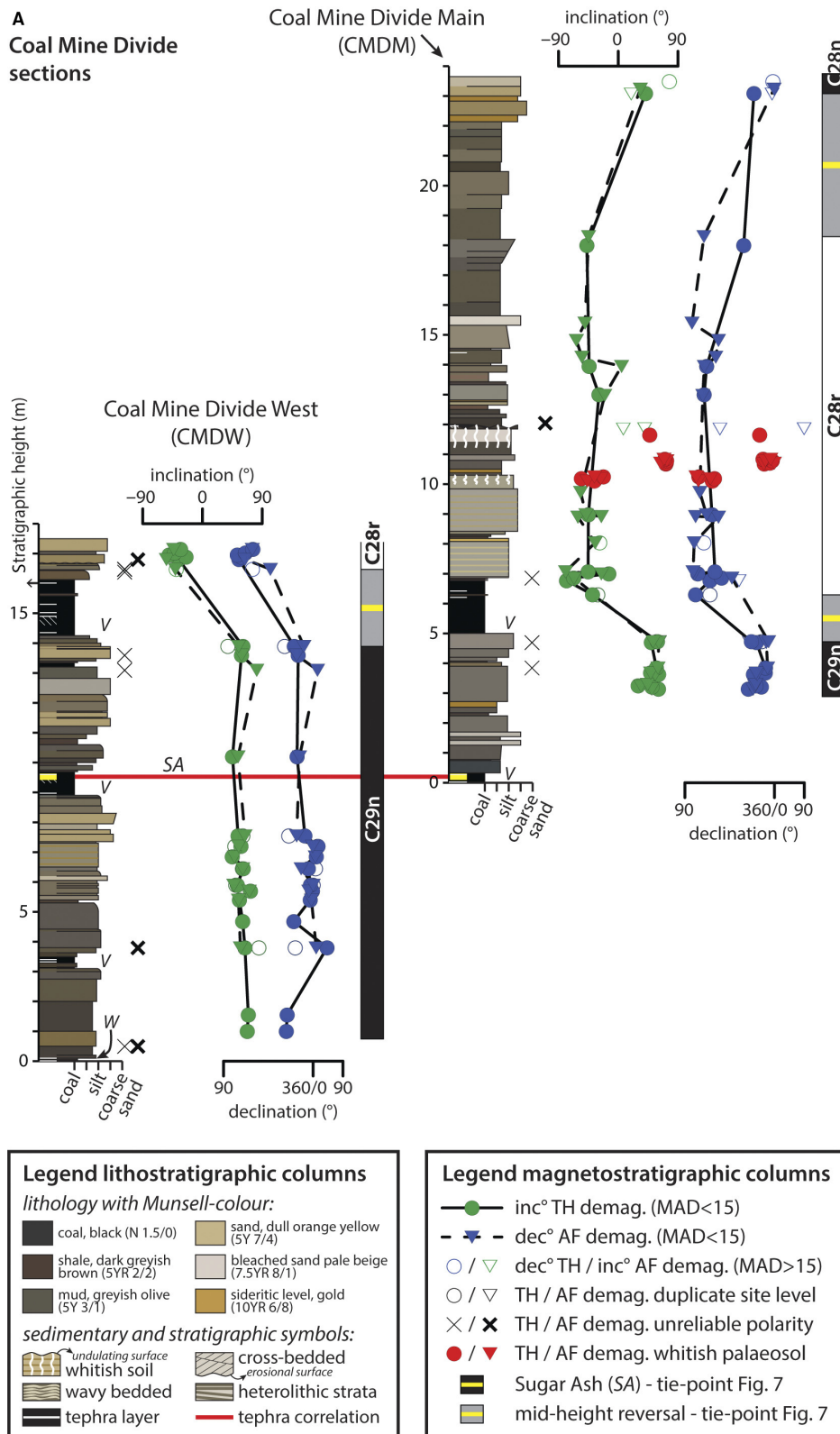
Fig. 2. Sedimentological logs and magnetostratigraphic columns of the sections. (A) Coal Mine Divide. (B) Rough Prong. (C) Radiotower part 1. (D) Radiotower part 2. (E) Horse Creek Road. Note: to improve visibility of the magnetostratigraphic reversals, samples in the magnetostratigraphic columns with a declination between 0° and 90° have been added to by 360° so that the declination range is set to 90 to 450 (90) degrees.
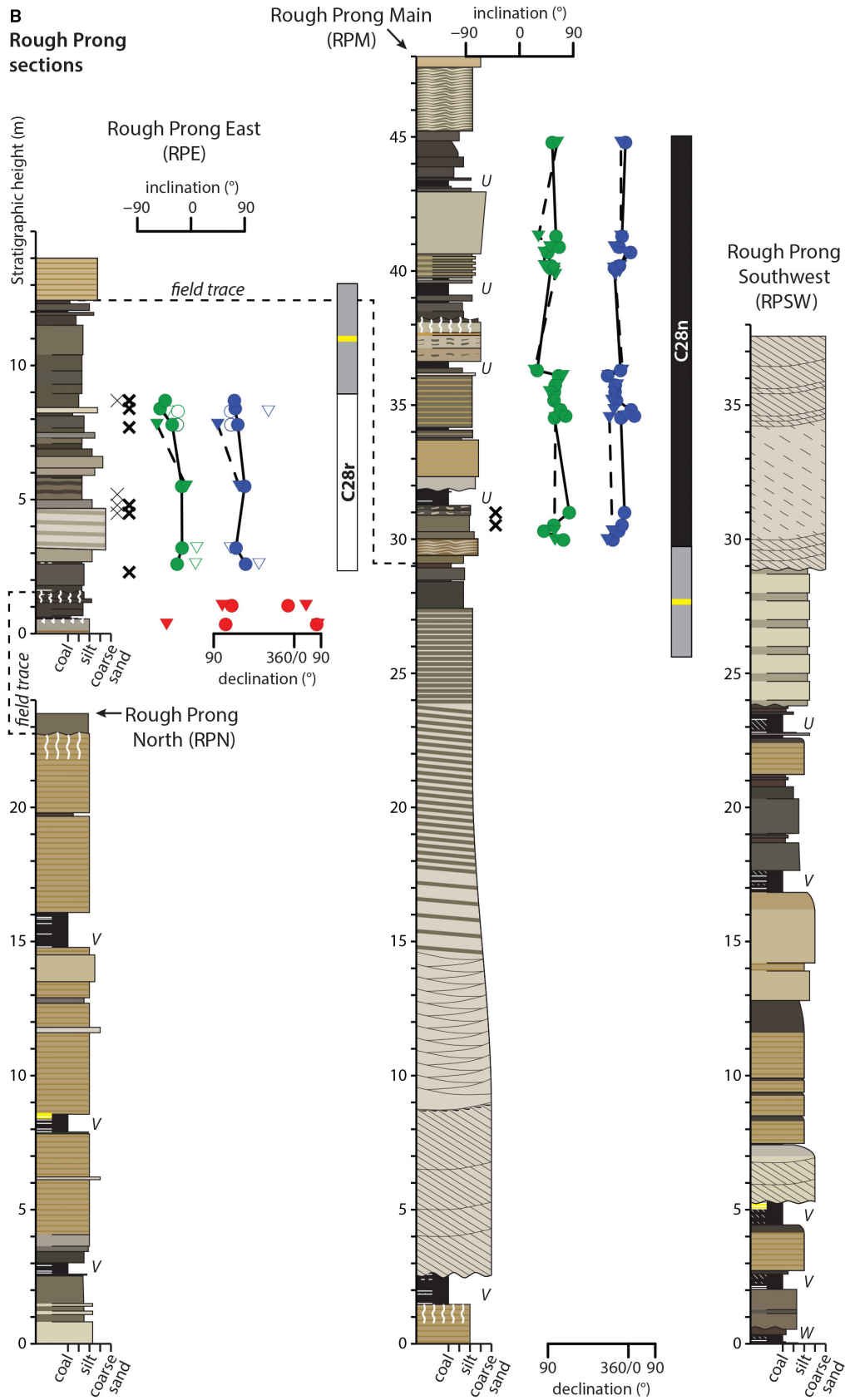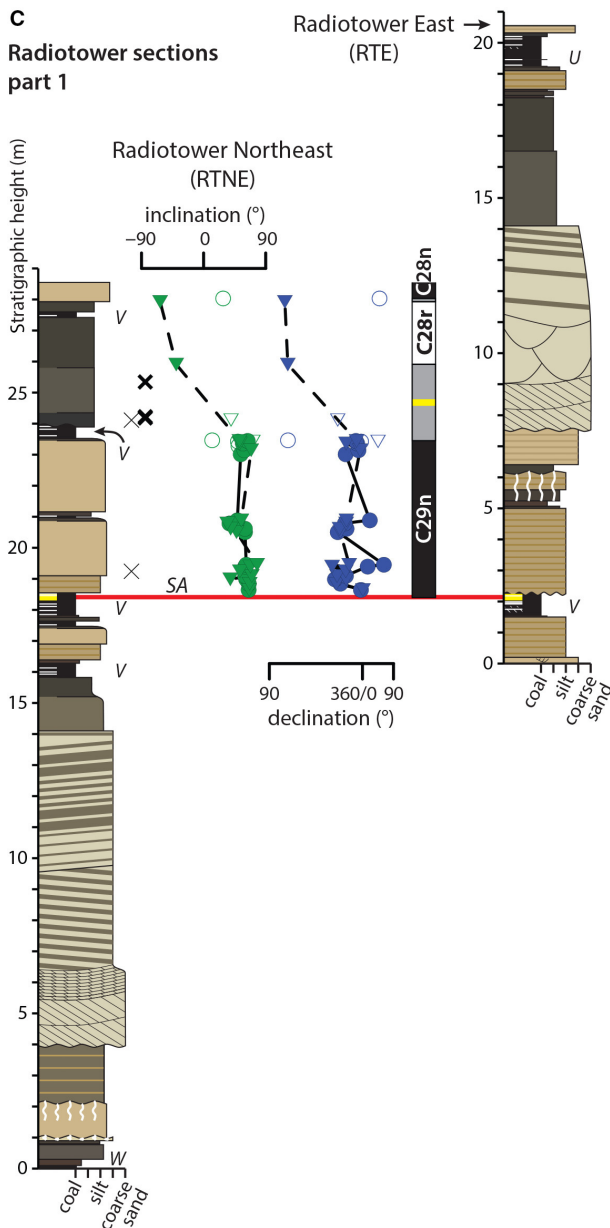
Fig. 2. Continued.

Fig. 2. Continued.

interval thus corresponds to C28r and the two recorded reversals to the C29n/C28r and C28r/C28n Chron boundaries.

Additional, more detailed, information on the demagnetization results is given in the Appendix S1, Data S1, Data S2 and in Fig. S1. The interpreted magnetostratigraphic data are provided in Tables S1 and S2. The raw palaeomagnetic data are available online in the data repository of this article.

Facies associations

Three facies associations are recognized in the Lebo Shale Member: (A) channel-splay, (B) valley-related, and (C) peat mire facies association. A description of the different facies within the facies associations along with their depositional interpretation is given below and summarized in Table 1. Figure 3 provides a field photograph of an outcrop in which the three Facies Associations A, B and C are identified. Facies-specific field photographs of the facies associations are provided in Figs 4, 5, and 6, respectively.

Facies Association A – Channel-splay

Description. Facies Association A (Fig. 4) is composed of Facies A1 (*ca* 20%), A2 (*ca* 10%) and A3 (*ca* 70%). Facies A1 consists of up to 10 m thick light-yellow-weathered sandstone bodies that are up to 0.25 km wide in cross-sectional dimension. From aerial view they show nearly straight ridges (Fig. 1C). The bodies consist of up to metre-scale trough-cross-stratified medium-grained sandstone sheets (Fig. 5C and D) gradually changing-upward to centimetre-scale trough cross-laminated and climbing ripple cross-laminated fine-grained to very fine-grained sandstone.

Facies A2 is represented by *ca* 1 to 15 m wide and *ca* 1 to 3 m thick, locally isolated, brownish-yellow-weathered concentric sandstone bodies with average total width–depth ratios of 4.8 ($\sigma = 1.4$, $n = 3$; Fig. 4B). The bodies consist of 10 to 30 cm thick concentric internal bedding composed of slightly muddy sandstone in the lower part and very muddy sandstone in the upper part (Fig. 4B).

Facies A3 is composed of *ca* 0.5 to 5.0 m thick brownish-yellow weathered, horizontally stratified packages consisting of decimetre to centimetre-scale silty sandstone (*ca* 80%) to mudstone (*ca* 20%) sequences that show a fining-upward trend (Fig. 4A). The silty sandstones are decimetre to centimetre-scale rippled

undetermined polarity (5.0%). The resultant magnetostratigraphy reveals a single reversed polarity interval with normal polarities stratigraphically both below and above. The lower normal polarities correspond to Chron C29n, because they represent the stratigraphic continuation of normal polarities recorded in the top part of the underlying Tullock Member that have previously been correlated to C29n by Noorbergen *et al.* (2018) in accordance with the $^{40}\mathrm{Ar}/^{39}\mathrm{Ar}$ radioisotope dating of Swisher *et al.* (1993) and Sprain *et al.* (2015). The reversed
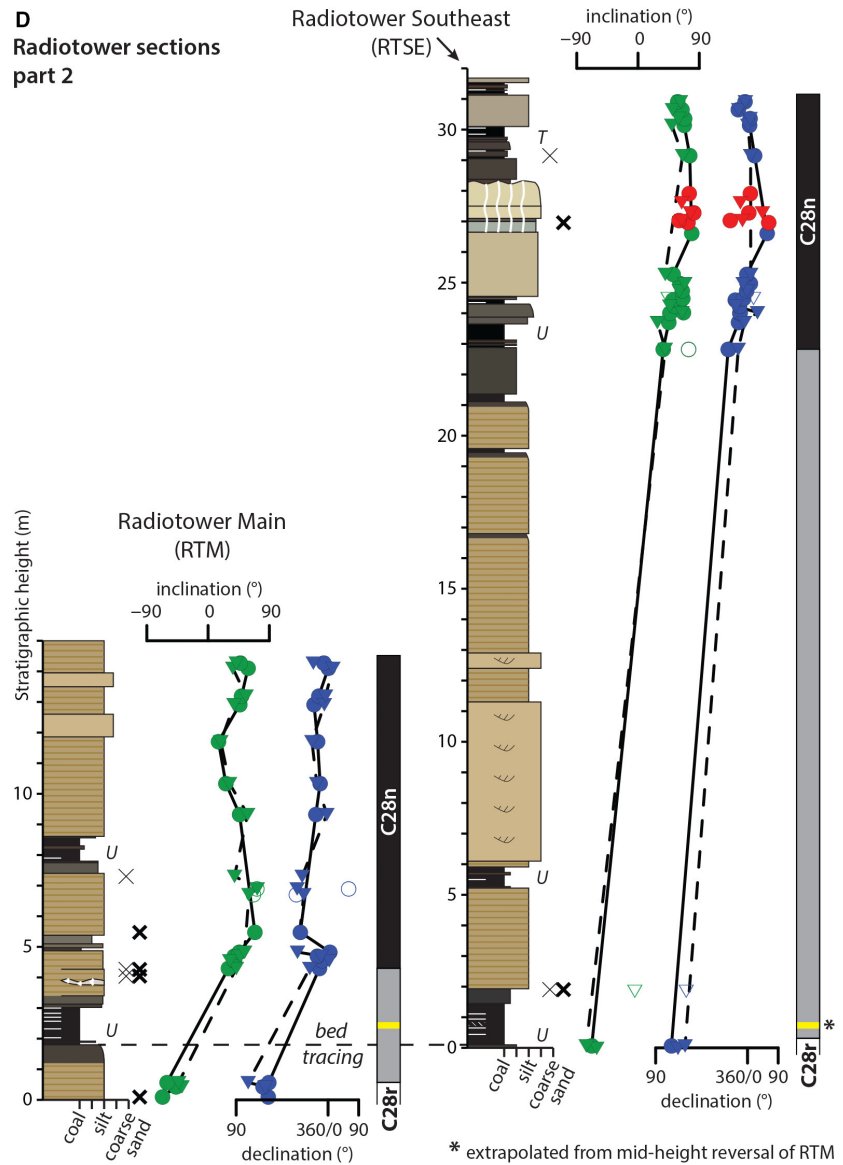
Fig. 2. Continued.

(Fig. 4E) and horizontally laminated. The mudstones contain decimetre to centimetre-scale horizontal laminations. The sand–mudstone sequences show kilometre-scale lateral extent. Locally mudstones can be up to 1 m thick. Within the horizontally stratified packages, up to 10 m wide lenticular intercalations of up to 2 m thick fine-grained sandstone bodies occur (Fig. 4A).

Decimetre-scale cross-stratified sandstone units of Facies A1 are found with a sharp contact on top of underlying facies. Laterally, sands of Facies A1 pass gradually into the laminated silty sandstones and mudstones of Facies A3. The concentrically bedded local sandstone deposits of Facies A2 have a sharp lower contact. Laterally, sediments in the upper part of Facies A2 pass gradually into those of Facies A3 (Fig. 4B).

Interpretation. The sharp bases, relatively coarse grain sizes compared to A3 and channelized geometries lacking major concave truncation-surfaces, point towards slightly erosive-based aggrading channels for the origin of Facies A1 and A2. Channel deposits of Facies A1 and A2 that laterally pass into the finer-grained deposits of Facies A3 indicate a crevasse-splay origin for the latter. The elongated cross-sectional nature, decimetre-scale cross-bedded sheets and low dispersive palaeo-flow (Fig. 1C) of Facies A1 are indicative of large-sized, low-sinuosity, sandy river channels (Rigby & Rigby,
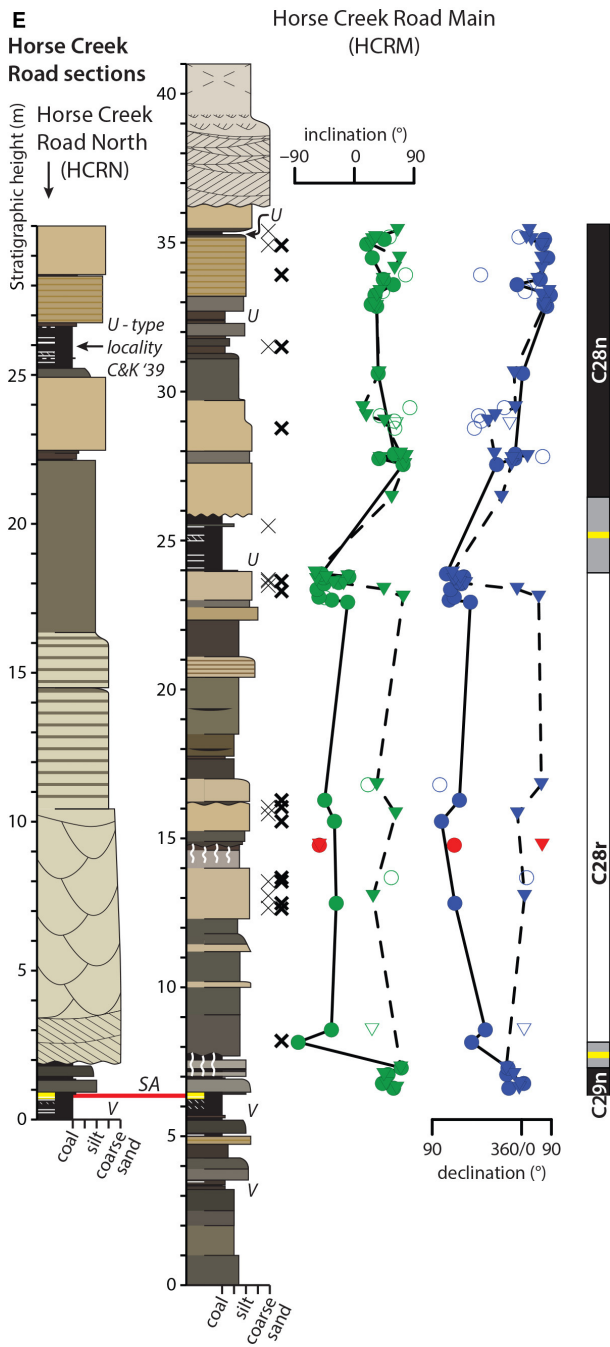
Fig. 2. Continued.

narrow channels with the filling composed of multiple individual beds (Gibling, 2006).

The grain-size range, sedimentary structures, and organic content of the horizontally stratified packages of Facies A3 suggest the presence of most crevasse-splay elements, i.e. crevasse-channel (lenticular sandstone intercalations), proximal to distal splays (respectively decimetre to centimetre-scale fining-upward sequences), and very distal splays (slightly laminated to structureless mudstones). The kilometre-scale lateral extent of the sand-prone (ca 80%) crevasse splay deposits indicate mature crevasse-splay systems. The high sand (relative to mud) fraction may be due to relatively low-accommodation, mainly offered by compaction of underlying peats and/or high amounts of sand in suspension during flood events (Burns *et al.*, 2017).

Facies Association B – Valley-related

Description. Facies Association B (Fig. 5) is composed of Facies B1 (*ca* 50%), B2 (*ca* 40%) and B3 (*ca* 10%). Facies B1 consists of up to 20 m thick, light-grey to grey-weathered heterolithic bodies (Fig. 6A and B) that are a maximum of 1 km wide in cross-sectional dimension and show multiple WNW–ESE oriented lenticular ridges from aerial view (Fig. 1C). The bodies consist of an up to 10 m thick, decimetre-scale cross-stratified, medium to fine-grained sandstone-dominated lower part (Fig. 5D) gradually changing-upward into a *ca* 10 m thick heterolithic upper part. The upper part is composed of low-angle inclined to horizontal decimetre-scale alternations of *ca* <40% fine-grained sandstone and *ca* >60% muddy sandstone (Fig. 5C). Within the decimetre-scale inclined sandstone–mudstone alternations, a few shallow truncation surfaces have been observed, laterally extending up to 200 m (Figs 4 and 6A). These contacts mark a slight <2° change in dip directions from underlying to overlying bedding. Up to metre-scale coal rafts and petrified tree trunks (Fig. 5F) occur within the bodies of Facies B1.

Facies B2 consists of up to 6 m thick mud-dominated units that are composed of decimetre-scale horizontal alternations between poorly structured, massive sandy claystone and millimetre to centimetre-scale, vaguely ripple laminated, muddy-sandstone layers (Fig. 5E). Centimetre to decimetre-scale pieces of petrified wood are generally aligned with the sandstone and mudstone bed surfaces of Facies B2 (Fig. 7B, C and D).

Facies B3 is characterized by up to 3 m thick white to light-grey weathered (bleached) heterolithic

1990). The sedimentation of sands in such channels possibly led to super-elevation with respect to Facies A3, initiating subsequent river avulsion and compensational stacking (e.g. Straub *et al.*, 2009; Hajek & Straub, 2017). The symmetrical cross-sectional nature, isolated occurrence and concentric internal bedding of Facies A2 argue for the presence of small-sized, relatively
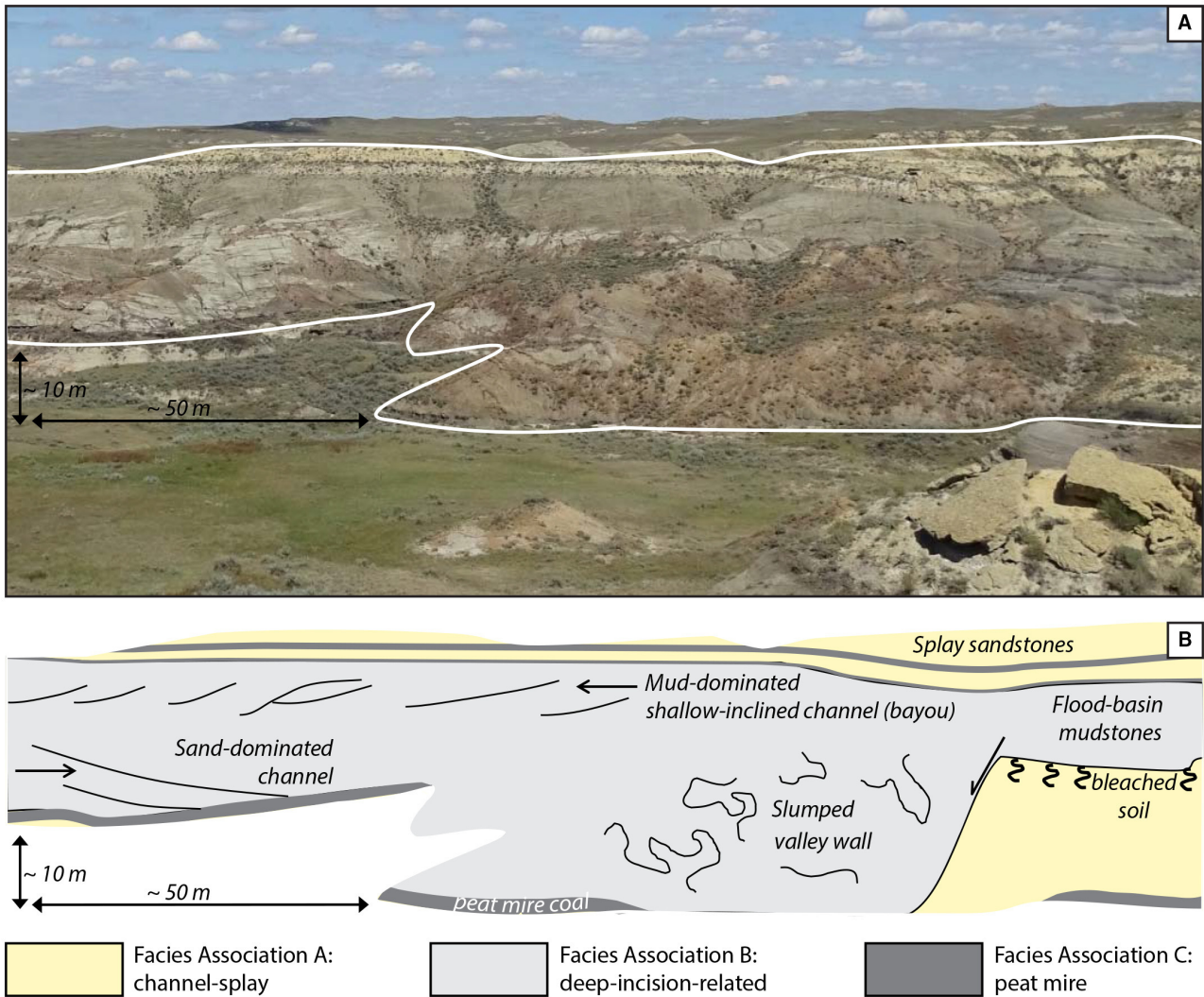
Fig. 3. (A) View to the north-west from the RP-M section showing the Lebo Shale Member in between the RP-N and RP-E sections, respectively, *ca* 1 km left and *ca* 500 m right outside the photograph (section locations in Fig. 1D). White line marks area interpreted in (B). (B) Sedimentary facies belonging to the three Facies Associations A, B and C identified for the Lebo Shale Member in north-eastern Montana (Table 1).

(clastic to coal) marker zones as these can be traced in the field over distances of several kilometres (Fig. 5H). When siliciclastic-prone, the horizons occur in the top parts of Facies Association A. When coaly, the horizons occur in the top of Facies Association C. Sandstone-prone horizons show white weathering, mudstone-prone horizons show light-grey weathering, and coal-prone horizons show bright-black weathering. Randomly oriented root traces, sometimes coalified, are common in the sandstones and mudstones. Many slickensides can be found in the mudstones. The sand-prone and mud-prone marker zones contain one or multiple gold (2.5Y 7/8) and/or dark purplish grey (5P 4/1) mottled

(up to 50%) zones and internally centimetre to decimetre-scale concretions may be present (Fig. 5I). Locally, just below the undulating top of Facies B3, an up to 20 cm thick, dark (10YR 1.7/1) sandy or muddy horizon occurs with centimetre-scale coaly patches, burrows and/or ash lenses (Figs 6E and 7A).

Heterolithic sandstone/mudstone bodies of Facies B1 are found with a sharp contact on top of other facies and along truncated sides of sand-dominated intervals. Such contacts are concave-up in case the truncated sediments belong to Facies B3 or to Facies Association A and C. The concave-up nature of the contact

Table 1. Facies associations of the Lebo Shale Member in north-eastern Montana.

Facies	Interpretation	Lithology, geometry and other contents	Sedimentary structures	Colour and present weathering	Unit boundaries
Facies Association A – Channel-splay					
A1	*Large-sized channel* with low-sinuosity, poorly confined flow, high clastic loads and rapid infilling leading to super-elevation and subsequent avulsion	Very fine, fine and medium-grained sandstone. Up to *ca* 10 m thick and *ca* 0.25 km wide sandstone bodies. Cross-sectional geometry shows elongated sheets. Aerial image shows a nearly straight ridge (Fig. 1C)	In lower part decimetre-scale trough cross-stratified sandstone. In upper part centimetre-scale trough cross-laminated layers and, climbing rippled cross-laminated layers	Greyish-yellow (2.5Y7/2), light-yellow weathering, locally indurated ribbons. Erosional resistant cover sandstone	Sharp erosional base, up to *ca* 4 m downward erosion, generally not through underlying coal. Generally a gradual transition when passing into overlying and juxtaposing A3
A2	*Small-sized channel* with confined flow, episodically high clastic loads and active to abandoned infilling	Muddy very fine to fine-grained sandstone. Concentric fill: 1–15 m wide and 1–3 m thick. Width–depth ratio *ca* 4.8	Sets of 10–30 cm thick concentric muddy sandstone fills. Set contacts marked by concentric cemented levels	Dull-orange-yellow (2.5Y 7/4), brownish-yellow weathering. Indurated at gold (10YR 6/8) concentric cemented levels	Sharply bounded along margins of concentric fill. Gradual transition with overlying A3
A3	*Crevasse-splay:* crevasse-channel, proximal, medial, distal to very distal splays	*Ca* 0.5 m to 5.0 m thick packages consisting of decimetre to centimetre-scale silty sand to mudstone fining-up sequences. Mudstones up to 1 m thick. Intercalation of up to 2 m thick lenticular fine-grained sandstone bodies. Small rootlets, leaves	Decimetre to centimetre-scale horizontal to slightly rippled cross-laminations. Centimetre to millimetre-thick cemented levels (variegated). Mudstones slightly laminated or structureless	Dark-yellow (2.5Y 6/4) silty sandstone, brownish-yellow weathering. Greyish-olive (2.5Y 4/3) mudstone, light-grey weathering	Gradual transition to overlying carbonaceous shale layers and coal seams. Sharply overlying coal seams
Facies Association B – Valley-related					
B1	*Fluvial valley* created by channel incision. Lower valley fill by low-sinuosity, high-energy meandering sandy channels. Upper and overfill of the valley by high-sinuosity low-energy muddy meandering bayous	Fine to medium sandstone-dominated lower part. Decimetre-scale alternations of very fine (>40%) and muddy sandstone (<60%) in upper part. Up to *ca* 25 m thick and *ca* 1 km wide sandstone bodies. Concave-up sides. Petrified trunks, peat rafts and organic residue in sandstones	Lower part: decimetre-scale trough cross-stratified sandstone that can be overlain by rippled cross-laminated muddy sandstone (up to 30% muddy laminae). Upper part: up to *ca* 60% mud in decimetre-scale horizontal and shallow inclined stratification. Inclined bedding up to *ca* 25°. Few truncation surfaces	Greyish-yellow (2.5Y 8/1) sandstone, light-grey weathering, locally indurated. Greyish-olive muddy sandstone (5Y 3/1), grey weathering, mud cracks. Aerial image shows a parabolic ridge (Fig. 1C)	Sharp erosional base, down-cutting, occasionally through underlying coal. Concave-up side, generally at boundary with Facies A. Gradual transition with overlying B2
B2	*Bayou flood-basin* receiving dominantly muddy sediments and driftwood from adjacent channel flooding	Up to *ca* 6 m thick mud-dominated units. Massive sandy clay (>60%) and muddy sandstone (<40%). Coalified root traces and slickensides in some levels. Petrified wood aligned with bed surface	Decimetre-scale alternations between slightly laminated, mainly massive sandy clay and slightly millimetre to centimetre-scale ripple laminated muddy sandstone	Dark-greyish-olive (2.5Y 2/1) to brownish olive (2.5Y 4/4) sandy clay/mud. Greyish-olive (5Y 5/2) muddy sandstone. 'Dirty-popcorn' weathering	Sharply overlying B3, at undulating surface between B2 and B3. Gradual transition if overlain by C1 and underlain by B1. Laterally passes into Facies C

Table 1. (continued)

Facies	Interpretation	Lithology, geometry and other contents	Sedimentary structures	Colour and present weathering	Unit boundaries
B3	*Inter-valley soil* with sporadically-preserved A, thick E and thin B horizons. Soil formation in between valleys took place during incision and confined valley flow	Up to 3 m thick light-coloured (bleached) zones, marking areas for several kilometres horizontal distance. Heterolithic: from sandstone, mudstone to coal. Many (coalified) root traces visible in sandstones and mudstones. Slickensides in mudstones	*Internal structures.* Poorly-developed, locally-concreted horizons with up to *ca* 50% mottles in bleached sandy matrix. Locally, just below undulating top, an up to *ca* 20 cm thick dark sandy or muddy horizon with coaly patches, burrows and small ash lenses	Pale-beige (7.5YR 8/1) whitish-weathered sandstone. Beige (7.5YR 6/1) light-grey-weathered mudstone. Gold (2.5Y 7/8) and dark purplish grey (5P 4/1) mottles and concretions. Brownish black (10YR 1.7/1) in top	Laterally passes into B1. Undulating surface at top of bleached zone or dark horizon. Frequently sharply overlain by B2 and sporadically sharply by D2. If darker horizon is overlain by D2 the undulating contact between them is barely visible
Facies Association C – Peat mire					
C1	*Shallow lacustrine*, locally (pond) or regionally (lake) inundated mire with little clastic input	Up to *ca* 0.5 m thick organic coaly shale to more laterally extensive massive carbonaceous (muddy) shale. Root traces, slicks and plant remains in coaly shale	Millimetre-scale laminated coaly shale. No clear sedimentary structures in massive carbonaceous shale	Dark-greyish-brown (5YR 2/2) coaly shale. Dark-greyish-olive (2.5Y 2/1) massive carbonaceous shale	Coaly shale lenses in B2 and C2. Coaly and carbonaceous shale sharply overlying B3, gradually overlying B2 and gradually underlying or overlying C2 or A3
C2	*Peat mire*, mostly extensive swamp environments dissected by low sediment-load peat-drained rivers	Lignite rank coal in up to *ca* 2 m thick coal seams consisting of centimetre to decimetre-scale alternations between bright (vitrain) bands with a conchoidal fracture (*ca* 75%) and dull-black dusty coal (*ca* 25%). Presence of amber. Lateral tracing of coal seams up to several kilometres	No sedimentary structures	Black dusty and bright coal to brownish black (10YR 1.7/1) bright coal	Relatively sharply overlying and underlying all other facies except for a more gradual transition with C1
C3	*Volcanic ashfall* from single volcanic eruptions in the western Cordilleran Thrust Belt. Preservation of ashfall layers particularly across low-relief mires	Up to *ca* 5 cm thick discrete ashy layers or ashy intervals. Grain-size range from very fine to coarse. Euhedral crystals. Ashy layers laterally pinch out and merge, up to lateral distances of tens of kilometres. Closely-spaced individual ashy layers make up ashy zones	No sedimentary structures	Pink beige (2.5YR 7/3) and pinkish light-grey (5YR 8/1) ash. Platy weathering of light-coloured, indurated ash intercalations within softer and darker-coloured coaly matrices	Sharply-bounded intercalations in coal or organic shales and mudstones

may abruptly end and become bedding-parallel when it reaches the top of a coal seam (Fig. 5A). Only a few sites show evidence for coal seams being truncated by a concave-up boundary (Fig. 5B). The upper inclined sand–mudstone alternations of Facies B1 pass laterally into the horizontally layered muddy sand–sandy claystone alternations of Facies B2 (Fig. 6A and B). Facies B2 becomes more dominated by massive sandy claystones some hundreds of metres away from the concave-up truncation of Facies B1, while it may gradually pass into coal seams *ca* 1 to 5 km from the truncation (Facies C1). The bleached zones of Facies B3 laterally thin towards the valley-fill of Facies B1. Stratigraphic boundaries between Facies B3 overlying Facies B2 and Facies Association C, are undulating (Figs 6E, 6H, 6I and 7A).

Interpretation. The sharp up to 15 m high concave-up boundaries of Facies B1, abruptly stopping on top of coal seams, argues for river channel incision creating fluvial valleys, while further incision was impeded or halted at underlying cohesive peat layers (Smith & Pérez-Arlucea, 2004; Van Asselen *et al.*, 2009). The decimetre-scale cross-stratified sand-dominated lower part of Facies B1 is indicative of lower-flow regime dune bedform aggradation (e.g. Miall, 1985), when post-incisional waning of flow velocities in the channel prevented bypassing of coarser sands. Likely, such waning flow velocities also caused relatively large transported organic components, such as peat slabs (later compacted to coal rafts) and tree trunks, to be contained and preserved within the sand dunes. The peat slabs probably were cut from underlying peat by the downward force of incision. During incision, the petrified tree trunks were uprooted from levées at times of bank-full discharge or they tumbled into the channel at times of over-saturated and/or critically steepened valley sides.

The up to 3 m thick bleached marker zones of Facies B3 laterally thinning towards the valley-fill of Facies B1 argues for intense soil leaching on inter-valley areas both during and after incision, when post-incisional sedimentation was restricted to the adjacent lower-lying valleys (e.g. Kraus, 1999; McCarthy & Plint, 1999, 2003). The mainly white to light-grey soil profiles, developed in the top parts of the yellowish-grey sandstones and mudstones of Facies Association A, point towards soil eluviation (E horizon). The centimetre to decimetre-scale gold and/or dark-purplish-grey mottled and locally concreted horizons may represent the illuviation in B horizons. Just below the undulating top of Facies B3, the dark organic-rich patchy horizons are likely indicative of the local preservation of humic topsoils (i.e. A and O horizons). The bright-black horizons with undulating tops that developed over coal seams which laterally pass into the valley-fills of Facies B1, are interpreted to be the result of inter-valley soil-leaching over peat parent material, although distinct soil horizons were not recognized in this lithology.

The horizontally stratified mud-dominated units of Facies B2 that overlie the undulating tops of Facies B3 and laterally pass into the shallow inclined sandstone and mudstone alternations of Facies B1 are interpreted in terms of a low-energy unconfined meandering bayou depositional system (e.g. Guccione *et al.*, 1999). The shallow truncation surfaces found within the muddy low-angle inclined upper deposits of Facies B1 may be formed by intra-pointbar erosion and rotation (Durkin *et al.*, 2015). The pieces of petrified wood horizontally aligned in the sandstone and mudstone bed surfaces of Facies B2 may reflect driftwood that drifted in the bayou flood-basin during overbank flooding. Any lack of tidal indicators (for example, ichnofacies and tidal-bundling) suggest that the inclined and horizontally heterolithic sandstone/mudstone deposits of, respectively, Facies B1 and B2 were mainly fluvial-influenced (Eberth, 1996). The sediments deposited on top of the valley fill (upper part Facies B1) and the laterally adjacent sediments deposited on top of the inter-valley soils (Facies B2) were named expansion surfaces by Martinsen *et al.* (1999). These authors explained these surfaces by abrupt increases in the accommodation space/ sediment supply ratio.

Facies Association C – Peat Mire
Description. Facies Association C (Fig. 6) is composed of Facies C1 (*ca* 10%), C2 (*ca* 80%) and C3 (*ca* 10%). Facies C1 include up to 50 m wide, *ca* 0.5 m thick, dark-greyish-brown, lenticular, coaly shale layers (Figs 7A and B) and massive, dark-grey carbonaceous (muddy) shale (top hill, Fig. 6A). The coaly shales are millimetre-scale laminated and contain millimetre to centimetre-scale vertical root traces, slickensides and millimetre-scale plant fragments.

Facies C2 consists of up to 2 m thick, brownish-black (10YR 1.7/1) to black coal seams (Fig. 7E to G). The coals consist of centimetre to
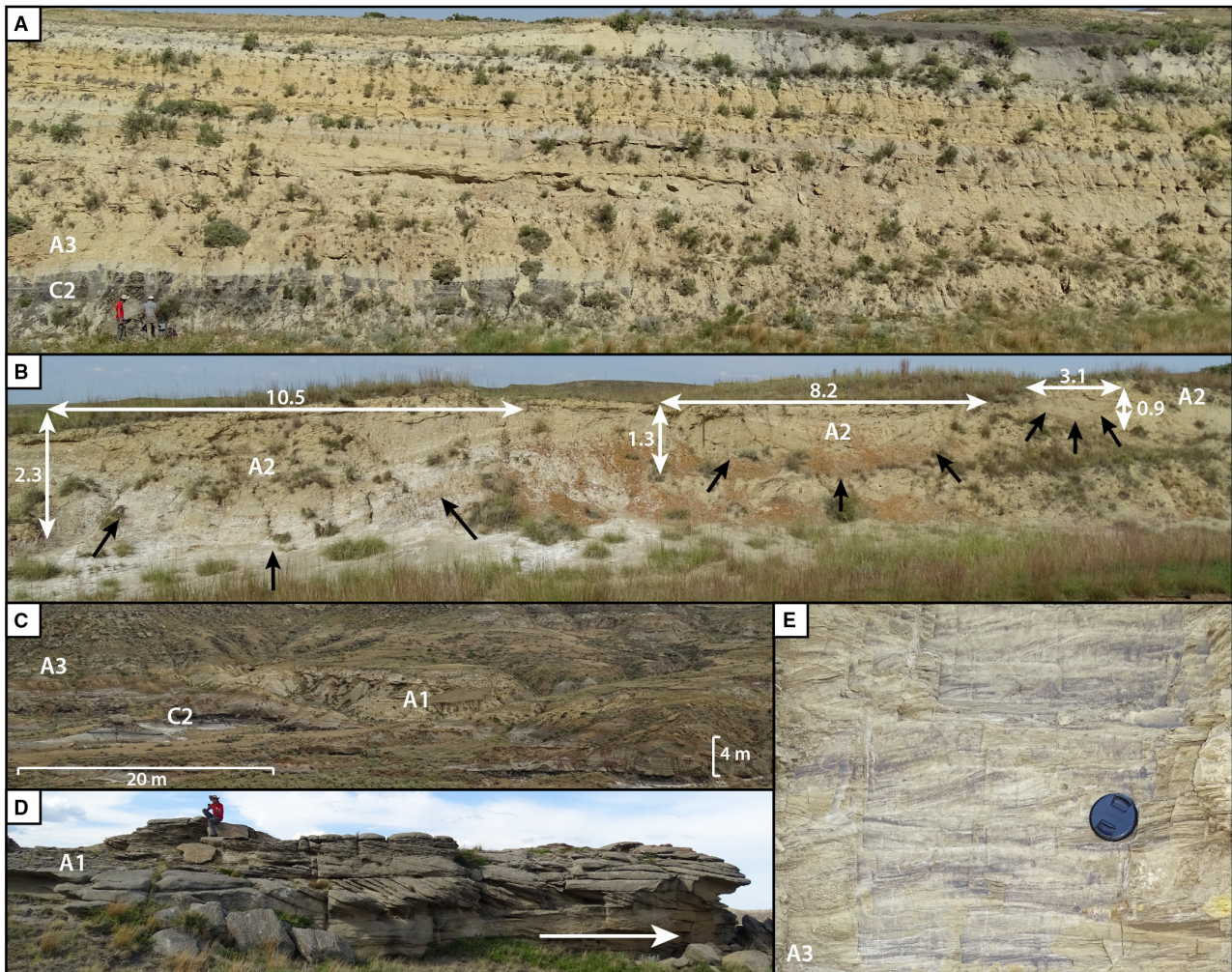
Fig. 4. Field photographs of Facies Association A – Channel-splay. A: Facies A3. Greyish-yellow crevasse-splay sandstones and mudstones resting on top of a coal seam in the upper part of the RT-M section. Indurated elongated sandstone ribbons in the middle representing crevasse-splay channel fills. Laterally discontinuous whitish layer at top reflects weak soil leaching in between splays. Persons for scale are *ca* 1.8 m tall. (B) Facies A2. Low-angle diagonal stacking of concentric small-sized channel sandstone fills. Average width-depth ratios *ca* 4.8. West-side of Highway 24, *ca* 500 m south of the RT-M section. (C) Facies A1. Yellow, indurated channel sandstone belonging in the lower part of the RP-SW section. The sandstone is *ca* 7 m thick on the right and thins to the left and passes laterally into splay deposits of Facies A3. (D) Facies A1. Trough-cross-stratified channel sandstone in the top of the RP-SW section. Arrow indicates palaeo-flow to (E). (E) Facies A3. Ripple cross-laminations marked by black organic matter in sandy mudstone splays. Lens cap for scale is 5.7 cm in diameter.

decimetre-scale alternations of bright (vitrain) bands with a conchoidal fracture (*ca* 75%) and dull-black dusty coal (*ca* 25%). Semi-spherical millimetre to centimetre-size pieces of amber are present in the coals.

Facies C3 is made up of up to 5 cm thick, pinkish beige (2.5YR 7/3) to pinkish light-grey (5YR 8/1), very fine to coarse ash layers or whitish ash-dispersal in a coaly matrix (Fig. 6G). The ash contains white-transparent, euhedral, very fine to coarse-grained crystals. Closely spaced individual ash layers may be clustered in zones up to 60 cm thick.

Lenticular coaly shales of Facies C1 are intercalated in Facies B2 and C2 (Fig. 6A). Coaly and carbonaceous shales of Facies C1 gradually overlie Facies B2, and gradually underlie and overlie Facies C2 and A3. Ash layers of Facies C3 are intercalated in Facies C1 and C2. Coaly and carbonaceous shales (C1) and coal seams (C2) sharply overlie Facies B3 and may gradually pass into Facies B2.
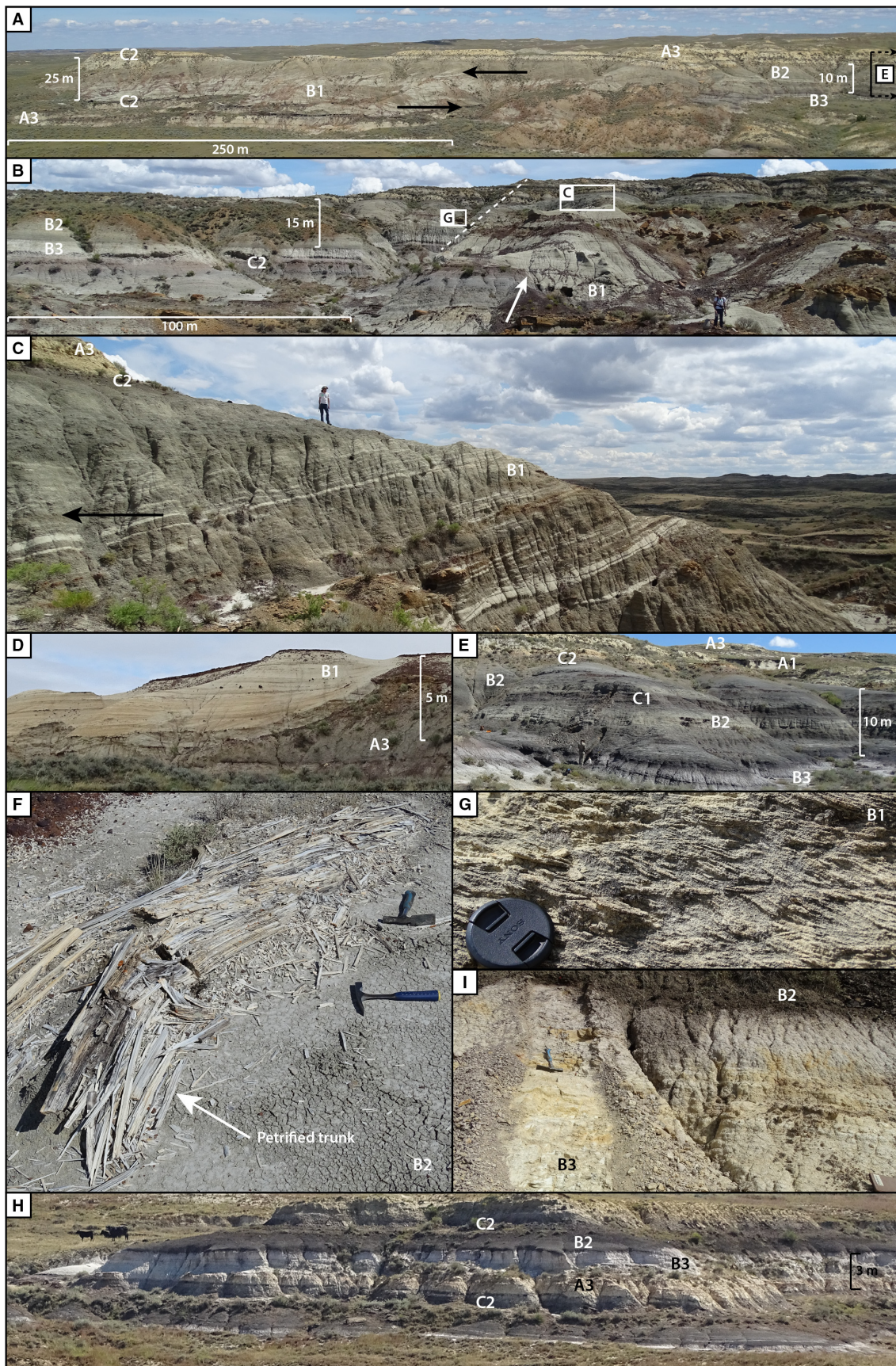
Fig. 5. Field photographs of Facies Association B – Valley-related. (A) Facies B1. Grey to light-grey fluvial valley fill units resting on top of a coal seam (C2) *ca* 500 m west of the RP-E section (panel E). Lower arrow shows point-bar accretion to the east in decimetre-scale cross-stratified sandstone-dominated part. Upper arrow shows point-bar migration to the west in low-angle inclined mudstone and sandstone decimetre-scale alternations. More detailed information on sedimentary facies of the same outcrop is provided in Fig. 3. (B) Facies B1. Grey to light-grey fluvial valley fill units in the lower part of the RT-NE section (dashed line). White arrow indicates truncation surface downward from the top of the #8-W coal (Noorbergen *et al.*, 2018), interpreted as the channel margin created during incision of the underlying peat layer. (C) Facies B1 (upper part). Low-angle inclined decimetre-scale mudstone and sandstone alternations interpreted as the muddy point-bar migrations of meandering bayous. Location photograph indicated by the white box in (B). (D) Facies B1. Channel cut bank *ca* 500 m north-west of the HCR-N section. (E) Facies B2. Grey to dark-grey decimetre-scale horizontal alternations between sandy claystone (dark-grey) and muddy sandstone (grey) at the RP-E section, representing bayou flood-basin sediments. (F) Facies B1 (upper part). Petrified trunk in mudstone possibly reflecting burial of driftwood after uprooting of partly-inundated trees during a bayou flood. Hammer for scale (length = 28 cm). (G) Facies B1 (lower part). Ripple cross-laminated sandstone reflecting waning energy of channel flow conditions. Black camera lens cover for scale (diameter = 5.7 cm). Location photograph indicated by white box in (B). (H) Facies B3. Regionally extensive bleached sandstone interpreted as the leached horizon of a soil that developed over Facies Association A on inter-valley areas during channel incision and valley filling. Undulating top surface represents the valley-related hiatus (blue lines Fig. 7). Location *ca* 1 km south-east of the RT-SE section. (I) Facies A3. Trench of bleached sandstone at the RT-SE section showing predominantly leaching-related white colours and mottling-related gold colours.

Interpretation. The coaly shale lenses of Facies C1 within the coal seams of Facies C2 may reflect the influx of clay from very distal splays in a shallow water peat mire environment. Coaly shale lenses of Facies C1 within the massive mudstones of Facies B2 may be interpreted as shallow water vegetated islands within a deeper water bayou flood-basin environment (e.g. Guccione *et al.*, 1999).

Coals of Facies C2 and carbonaceous shales of Facies C1 laterally passing into the massive mudstones of Facies B2 point to a backswamp environment adjacent to the bayou. Coal seams of Facies C2, that are laterally continuous, not being interrupted by interfingering channels of Facies Association A, and that do not pass into the massive mudstones of Facies B2, were likely formed in regionally extensive peat mires in which drainage was mainly diffusion-dominated in the absence of well-defined channels (Whitfield *et al.*, 2009). The centimetre to decimetre-scale alternations between dull-black and bright-black coal may reflect wet–dry cycles, respectively (Potter *et al.*, 2008; Holdgate *et al.*, 2016; Korasidis *et al.*, 2016).

Within Facies C1 and Facies C2, the intercalation of discrete ash layers and zones composed of euhedral, very fine to coarse-grained crystals indicates a volcanic ashfall (tephra) origin of Facies C3 (Bohor & Triplehorn, 1993). The discrete ash layers may reflect tephra preservation in low-relief, possibly drowned peat mires while the ash dispersal intervals may point to rapid peat-forming conditions in raised mires (Triplehorn *et al.*, 1991).

Fence panel

Chronostratigraphic markers

Three major chronostratigraphic markers have been used for correlation of the sections. The stratigraphically lowest marker is a pinkish light-grey (2.5YR 7/2), up to 3 cm thick, medium to coarse-grained ashfall layer containing euhedral-shaped and transparent sanidine crystals. It is consistently found in the top part of a *ca* 1 m thick coal seam in the upper part of the C29n magnetochron and can be traced over tens of kilometres. Sieving of grain-size fractions in the laboratory shows that this tephra mainly has a grain-size range of 250 to 550 μm, whereas grain sizes of other tephras in the study area range between 62.5 μm and 200 μm. The coarse tephra layer is unique in its grain size and represents a key layer for stratigraphic correlation. The transparent light-grey crystals and the grain size resemble crystals of granulated sugar. Therefore, this tephra was named 'Sugar Ash'.

The second marker is the C29n/C28r geomagnetic polarity reversal. This polarity reversal occurs *ca* 6 m above the Sugar Ash at Coal Mine Divide West (CMD-W), Coal Mine Divide Main (CMD-M) and Radiotower Northeast (RT-NE). At CMD-W and CMD-M, the C29n/C28r reversal occurs within a 1 to 2 m thick coal seam (Figs 3A and 8), labelled the U-coal by Collier & Knechtel (1939) (Fig. 1D). In the southernmost
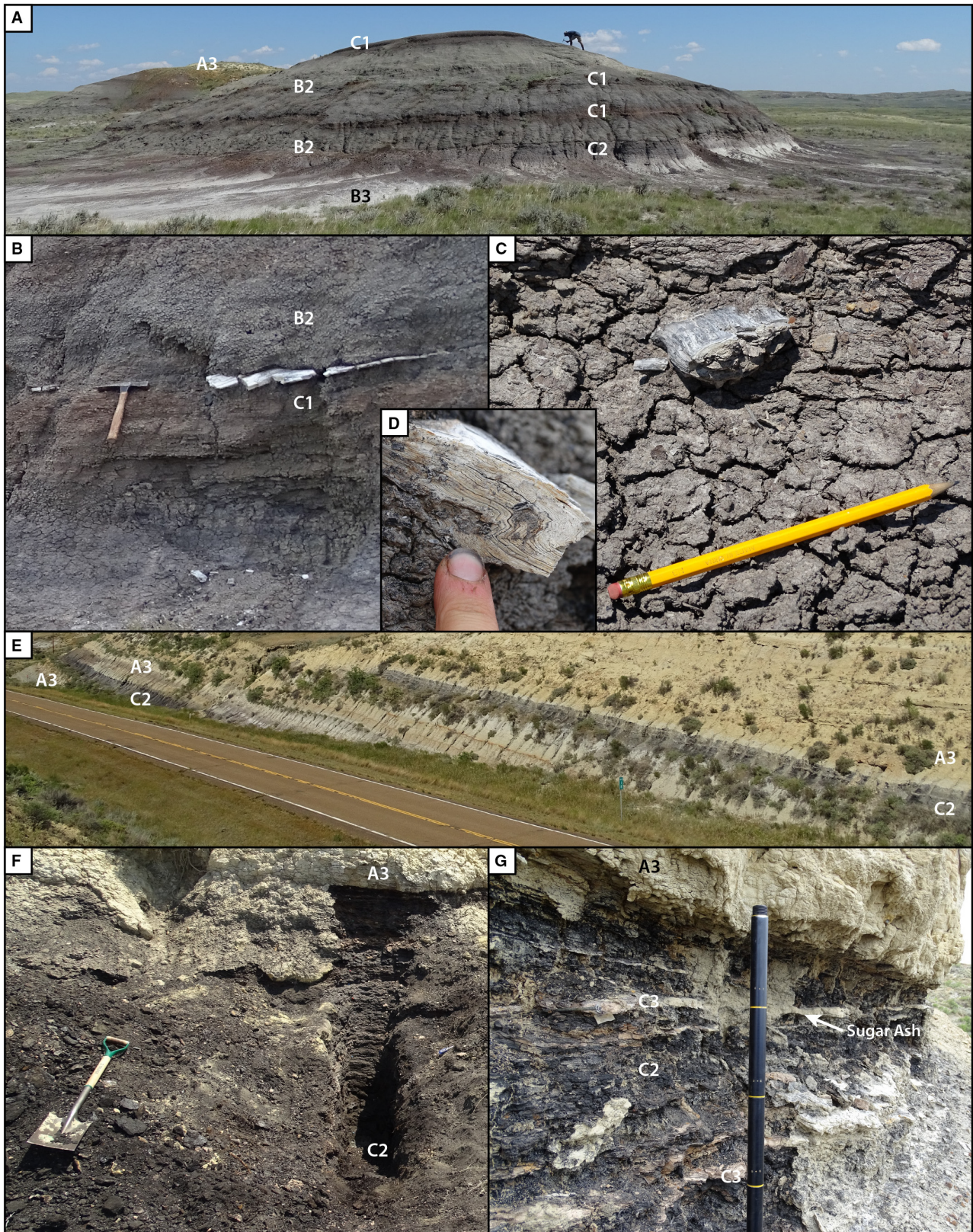
Fig. 6. Field photographs of Facies Association C – Peat Mire. (A) Facies C1. Several lenticular dark-greyish-brown coaly shale layers intercalated in Facies B2 *ca* 500 m east of the CMD-W section. Layers may have been locally formed on shallow-water vegetated islands during decreasing bayou water depths. (B), (C) and (D) Facies C1. Pieces of wood parallel to bedding of Facies B2 reflecting the settling of driftwood that was introduced in the flood-basin after high discharge events. Hammer (*ca* 28 cm), pencil (*ca* 18 cm) and fingertip (ca 3 cm) for scale. (E) Facies C2. Two coal seams of the U-coal zone exposed along Highway 24 at the RT-M section. Strong lateral continuity reflects a palaeo-environment dominated by peat formation in the absence of major clastic sediment supply. Green traffic sign for scale (height *ca* 2 m). (F) Facies C2. Trench in a 2 m thick coal seam in the upper part of the V-coal zone at the CMD-W section; previously labelled the U-coal bed by Collier & Knechtel (1939). Shovel for scale (length *ca* 125 cm) (G) Facies C3. Coal seam of the V-coal zone at the RP-SW section with several light-coloured ash layers containing euhedral crystals interpreted as volcanic ashfall. Yellow bars on Jacob Staff are spaced 0.2 m. At 0.2 m below the top of the coal, aligned with a yellow bar on the Jacob Staff, is the characteristic 'Sugar Ash'.

part of the transect, at Horse Creek Road Main (HCR-M), the C29n/C28r reversal occurs in the lower part of a clastic interval directly above a whitish mature, 0.75 m thick palaeosol, *ca* 1.5 m above the Sugar Ash (Figs 3E and 8). The Horse Creek Road sections are located in the type area of the U-coal of Collier & Knechtel (1939) (Fig. 1). The U-coal at HCR-M occurs at 17 m above the C29n/C28r reversal, at the stratigraphic position of the C28r/C28n reversal (Fig. 7).

The stratigraphically highest marker is the C28r/C28n geomagnetic polarity reversal. It occurs in a carbonaceous shale and mudstone interval, *ca* 20 m above the U-coal of Collier & Knechtel (1939) at Coal Mine Divide Main (CMD-M), Rough Prong East (RP-E) and Rough Prong Main (RP-M) (Fig. 7). At Radiotower Main (RT-M), Radiotower Southeast (RT-SE) and Horse Creek Road Main (HCR-M), the C28r/C28n reversal occurs within a 1 to 2 m thick coal seam that was mapped as the U-coal by Collier & Knechtel (1939) (Fig. 7).

Coal nomenclature: The U-coal revisited
Correlation of the polarity reversals shows that the U-coal of Collier & Knechtel (1939) in the north and the U-coal of Collier & Knechtel (1939) in the south cannot be the same (Figs 1D and 8). They are different coals stratigraphically separated from one another over a time interval that encompasses the entire Chron C28r, *ca* 224 kyr (Dinarès-Turell *et al.*, 2014). Thus, the mapping of the U-coal bed in the study area by Collier & Knechtel (1939), is inconsistent with respect to current chronostratigraphic results and needs to be revised. In updating the U-coal labelling across the study area, the underlying V-coal and overlying T-coal also have to be re-assigned. On the premise of keeping the original U-coal label in its type area (Collier & Knechtel,

1939), the U-coal in the south of the fence panel discussed here, at the stratigraphic position of C28r/C28n, keeps that labelling. It is now, however, defined as a zone consisting of multiple closely spaced coals (Fig. 7). As a result, the U-coal as mapped by Collier & Knechtel (1939) in the north of the fence panel, at the stratigraphic position of C29n/C28r, is now untenable. In that region, this original U-coal is included in the V-coal zone consisting of a cluster of three coal seams with the Sugar Ash in the middle seam (Fig. 7). The V-coal zone overlying the upper part of the W-coal zone (i.e. #8-W coal) is consistent with Noorbergen *et al.* (2018). The T-coal zone is re-assigned to the coal zone above the bleached palaeosol at RT-SE. The V-coal and T-coal were not mapped in the study area by Collier & Knechtel (1939).

Coal correlation
Chronostratigraphic correlation of the three markers (Fig. 7) shows that some coal seams can be correlated along the whole transect of the fence panel while others cannot. The basal coal in the upper W-zone shows lateral continuity, except just south of RT-NE where it is truncated by a sandstone complex over a distance of *ca* 500 m (white arrow, Fig. 5B). Overlying the W-zone, in the V-zone, two coal seams also show lateral continuity: the coal seam of the Sugar Ash and the coal seam below that. Correlation of the C29n/C28r reversal shows that the revised U-coal of Collier & Knechtel (1939), now in the upper V-zone, is laterally discontinuous. This coal is *ca* 2 m thick in the north. To the centre of the fence panel, it becomes thinner, with a thickness of 0.5 m. It is absent in the south of the fence panel at the contact of a whitish palaeosol (Facies B3) disconformably overlain by clastic fluvial deposits (Facies B2).
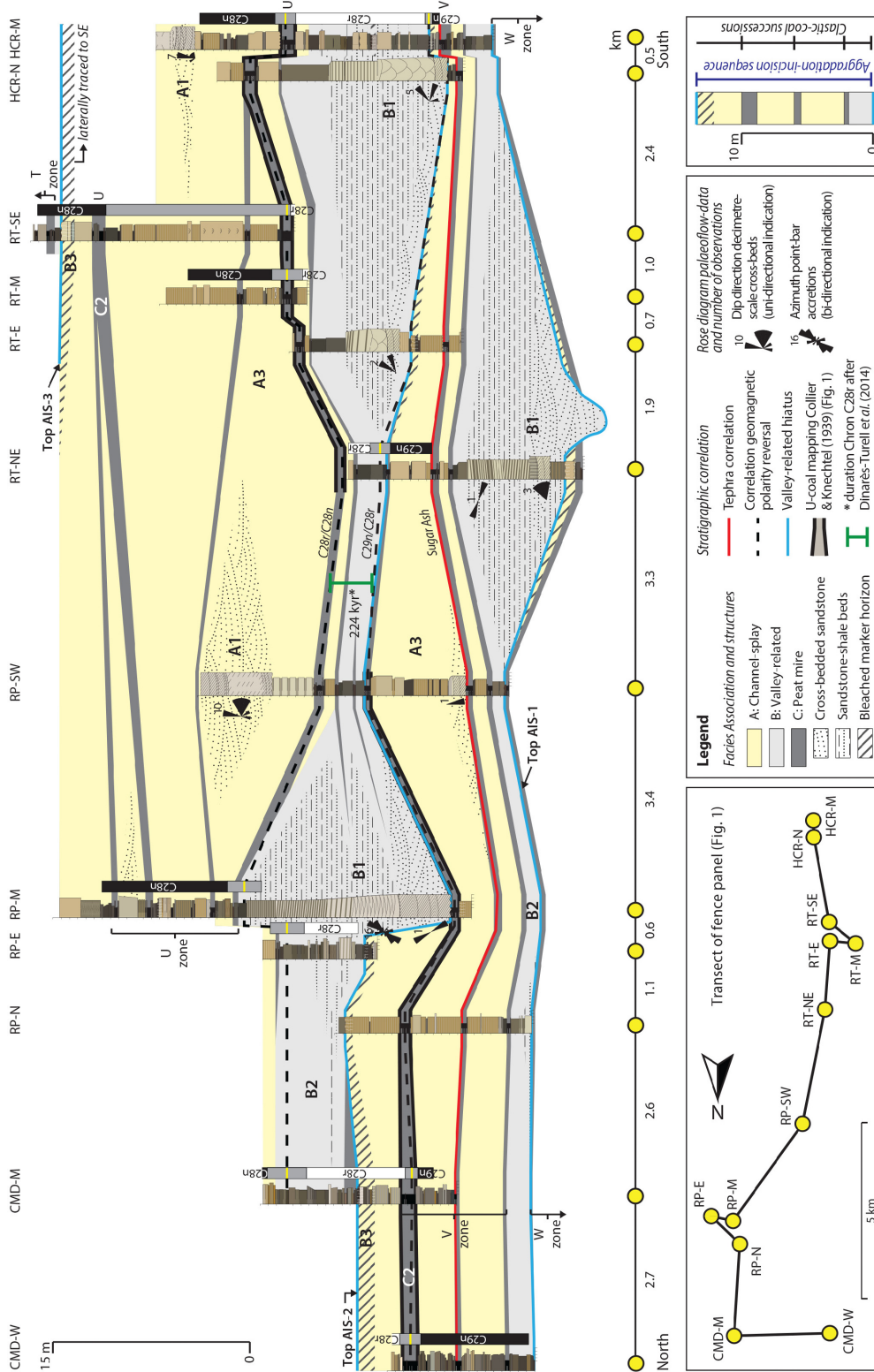
Fig. 7. Stratigraphic fence panel of the Lebo Shale Member along the north–south transect (Fig. 1). Vertical positions of sections are calibrated using the optimization approach described in the text. Sections are correlated using the Sugar Ash (red solid line) and the C29n/C28r and C28r/C28n polarity reversals (black dashed lines). The coal seams mapped as the U-coal bed by Collier & Knechtel (1939) are bracketed by solid black lines. Facies Associations A (light-yellow), B (light-grey) and C (dark-grey) are shown. Lateral development of channel and valley fills is indicated with dots (sand) and dashes (mud). Rose diagrams of palaeo-flow data are provided left of sections where measured. Time stored in the C28r sediment interval indicated left of green vertical scale bar is based on Dinarès-Turell *et al.* (2014). The figure shows ten 100 kyr scale coal–clastic successions and three 400 kyr aggradation–incision sequences (AIS). Valley-related hiatal surfaces of the three AIS are indicated by blue solid lines.

Correlation of the C28r/C28n reversal shows that the stratotype U-coal of Collier & Knechtel (1939) is also laterally discontinuous. This coal is *ca* 2 m thick in the south. To the centre of the fence panel, it becomes thinner with a thickness of 1 m. It is absent in the north of the fence panel where, instead, massive mudstones of Facies B2 occur. Laterally continuous coal seams are shown above the C28r/C28n reversal (upper part, Fig. 7). Above the C28r/C28n reversal, additional chronostratigraphic correlations are lacking. Coal correlations in this interval are mainly based on lithostratigraphic interpretations that are locally supported by field tracing of coals and bleached zones.

Successions and sequences

The new chronostratigraphic correlations allow for further interpretation of the stratigraphic architecture of the sediment successions and sequences (Table 1) at metre-scale resolution (Fig. 7). Two scales of alternations are identified. The first are *ca* 5 m thick coal–clastic aggradational successions (CCS) consisting of a peat mire facies association (C) overlain by a channel-splay or valley-related facies association (A or B). A total of ten CCS are identified in the fence panel.

Superimposed on the *ca* 5 m thick CCS are *ca* 15 m thick aggradation–incision sequences (AIS). At the base these sequences start with the aggradation of Facies B1 and B2 deposits on top of *ca* 20 m thick valley-base and inter-valley undulation surfaces. Overlying Facies B1 and B2, are the aggradations of *ca* three to four CCS. The top of the AIS are in the last CCS where the aggradation stops at the undulating top surface of a bleached zone (Facies B3) laterally passing into the valley-base of Facies B1 representing the incision. A total of three AIS are identified in the fence panel (Fig. 7). The lowermost AIS (AIS-1) only shows its uppermost part. The overlying AIS-2 has the most complete architecture with 5 to 15 m aggradation. AIS-2 is laterally truncated in its top part by two valleys filled by Facies B1 and related to soil zones of Facies B3 occurring in between the valley-fills on elevated platforms. On top of AIS-2, AIS-3 is composed of 15 to 20 m aggradation in the south where it is covered by a bleached zone in the top (Facies B3). To the north, the soil formation zone exceeds the upper fence panel margin because the full thickness of AIS-3 is not exposed in that area. Chron C28r comprises the uppermost aggradation phase of AIS-2, the incision phase of AIS-2, and the lowermost aggradation phase of AIS-3 (Fig. 7).

A first-order quantification of minimal incision depth is calculated by the difference between the thickness of the full valley fill (Facies B1 and B2) at the place of deepest incision and the thickness of Facies B2 above the inter-valley soil (Facies B3). The latter locality has seen significantly less erosion during the incision phase. The authors cannot account for differences resulting from sand/mud compaction and depositional thickness due to palaeo-topographic effects at the time of deposition. The minimal incision depth of AIS-1 is 8.3 m and AIS-2 is 5.1 m.

Compensational stacking patterns

Both at the scale of CCS and AIS compensational stacking patterns are observed (Fig. 7). Facies become thicker at places where underlying facies were thinner and vice versa. For the successive CCS, these patterns are shown by the Facies Association A sediments. Examples are in the V-coal zone of RP-SW and in the U-coal zone of RP-M, RP-SW, RT-M and RT-SE (Fig. 7). The compensational stacking pattern for AIS is observed between RP-SW and RT-NE. Here Facies Association B deposits of AIS-3 thin from the north and from the south on top of thick Facies Association B deposits of AIS-2 that are situated in the central part of the panel. These lateral thickness variations of facies likely reflect the effect of palaeo-topography on sedimentation. The lateral extent of compensational stacking for CCS is at *ca* 10 km and for AIS at *ca* 15 km (Fig. 7), indicating that sedimentation evened out over these distances.

With the compensational stacking of the CCS, coals (Facies C2) do not gradually pass into lateral clastics of Facies Association A. This suggests the absence of syndepositional channel-belts of Facies A1 coeval with peat formation. The coals in the lower U-zone do gradually pass into the massive mudstones of Facies B2 (Fig. 7), suggesting that these facies co-existed.

Time control and duration

The two geomagnetic polarity reversals spanning chron C28r and the Sugar Ash provide constraints on durations of coal–clastic successions (CCS) and aggradation–incision sequences (AIS). The duration of chron C28r is 291 kyr in the Geological Time Scale 2012 based on astronomical tuning (Vandenberghe *et al.*, 2012). More recent estimates on the duration of C28r arrive at 224 kyr
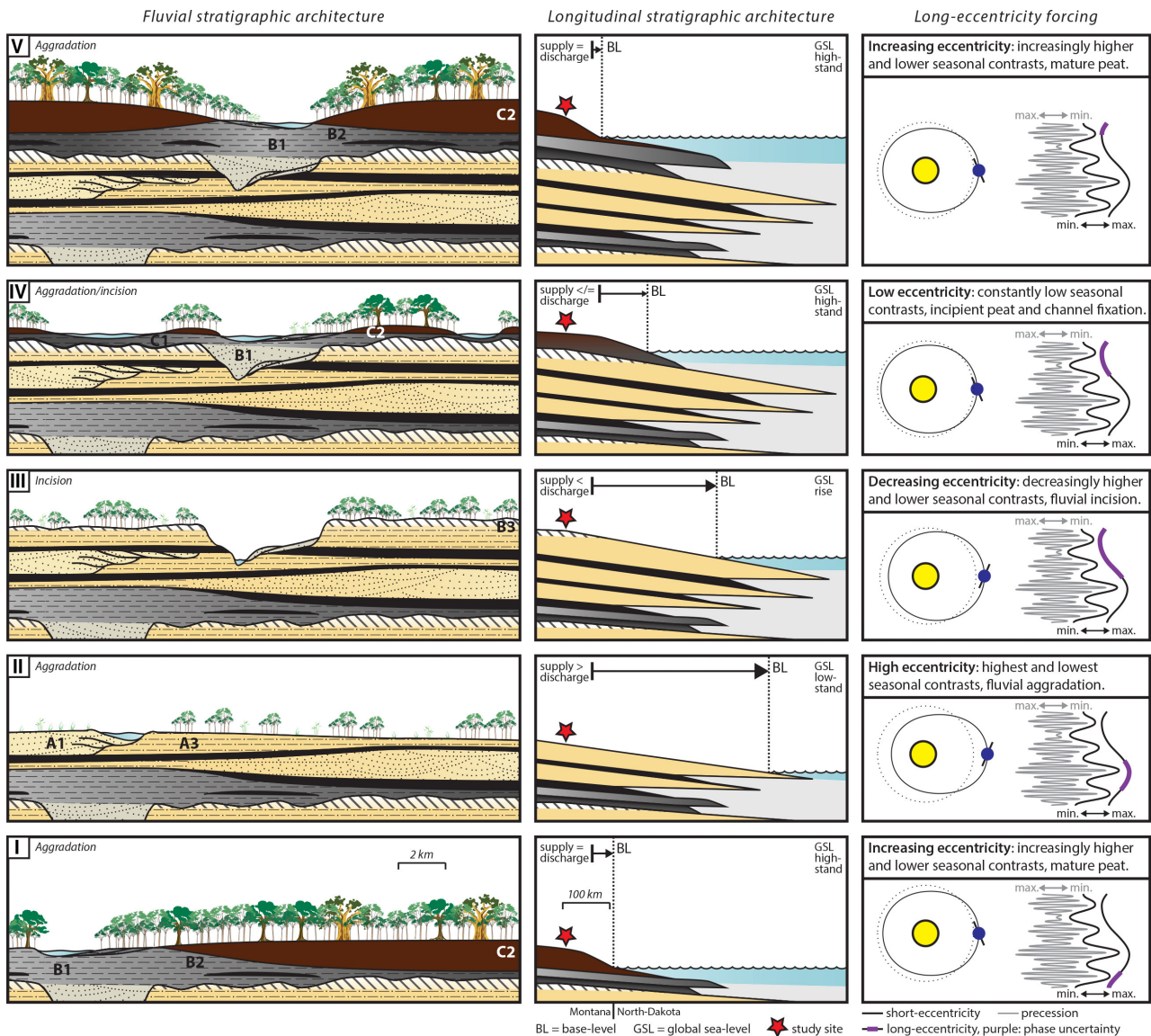
Fig. 8. Five-stage conceptual stratigraphic model illustrating the role of long-eccentricity-scale climate change in building aggradation–incision sequences (AIS) in the Lebo Shale Member in north-eastern Montana (left panel) and in building down-gradient lower Fort Union stratigraphy in the Williston Basin (middle panel). Phase relations with long (purple) and short (green) eccentricity and precession, including time-uncertainty, are shown on the right. A detailed description of each stage is provided in the text.

by combining several astronomically tuned chronologies in Spain, the Atlantic, and the Pacific (Dinarès-Turell *et al.*, 2014), at *ca* 358 kyr based on ^{206}Pb/^{238}U radioisotope ages of tephras in the Kiowa Core of the Denver Basin (Colorado, USA) in combination with a revised magnetostratigraphy (Clyde *et al.*, 2016), and at 252 kyr using ^{40}Ar/^{39}Ar data of two ash-layers below (= the Sugar Ash) and above C28r in the Fort Union Formation, Garfield County, Montana (Sprain *et al.*, 2015). Although these estimates range from 224 to 358 kyr, it is important to note

that chron C28r corresponds to a 405 kyr eccentricity minimum as evident from the integrated stratigraphic framework of Dinarès-Turell *et al.* (2014). A closer look at the short-eccentricity scale further reveals that C28r apparently starts in a 100 kyr eccentricity maximum or on the transition from a 100 kyr maximum to minimum, and that C28r contains two 100 kyr minima (Fig. S2A–C; green arrows) and the maximum in between.

The above implies that the valley-related Facies Association B sediments of AIS-3 are deposited somewhere during the 400 kyr minimum. To

develop a conceptual model of long-eccentricity forced fluvial stratigraphy, it is relevant to locate the moment of incision followed by aggradation in relation to this 405 kyr long cycle. Based on Fig. S2 it seems that the incision of AIS-2 occurs either during the transition of a long-eccentricity maximum to a minimum or in the minimum itself.

Uncertainties in the exact position of C28r chron boundaries (i.e. grey intervals) in the Lebo Shale do not allow to decipher the exact phase-relation of the sedimentary succession with the 100 kyr short-eccentricity cycle, as known from the marine realm (Dinarès-Turell *et al.*, 2014). Besides, it is important to note that the 100 kyr eccentricity cycle in contrast to the 405 kyr cycle is not reliably represented in the astronomical solution, due to chaotic behaviour of the Solar System (Laskar *et al.*, 2004). Therefore, the timing of incision and the subsequent onset of valley infill with respect to the short-eccentricity-cycle remains elusive.

DISCUSSION

Controls on the aggradation–incision sequences (AIS)

Tectonics
At 400 kyr timescales flexural foreland-basin tectonism may exert a control on building reciprocal fluvial stratigraphy (Miall, 2014). Foreland-basin flexural tectonism is the flexural behaviour of the foreland lithosphere in response to successive stages of orogenic loading and unloading (Beaumont, 1981; Catuneanu *et al.*, 1997). As a result, creation and disappearance of accommodation space and associated sequence patterns will be out of phase between the proximal and distal regions of the foreland basin where separation is marked by a foreland system hinge line. Based on bentonite and ammonite-zone correlations in Campanian to Palaeocene strata in the Western Interior Foreland Basin (particularly in the Canada area), Catuneanu *et al.* (2000) made a reconstruction of the hinge line position during seven consecutive time intervals from the Campanian to Palaeocene, providing an indication of *ca* 3 Myr stages of foredeep migration. Sediments of the Lebo Shale Member were deposited in the study area when the hinge line was located *ca* 150 km westward (Catuneanu *et al.*, 2000). The associated westward retreat of the foredeep towards the Cordilleran orogeny during the early Palaeocene may reflect an episode of orogenic quiescence (Catuneanu *et al.*, 2000). This quiescence is in agreement with eastward advancing Laramide thrust-sheets later in time, representing the middle Palaeocene Bighorn Uplift and the early Eocene Black Hills uplift (Belt, 1993; Belt *et al.*, 2004).

Tectonic control on foreland accommodation, with its associated positive or negative space for sedimentation, may overwhelm time-overlapping orbital controls (i.e. long to very long eccentricity cycles) or it may remove stratigraphy that was formed by shorter-term controls (for example, short-eccentricity cycles or autogenic processes) due to upwarping. Acting on 1 to 10 Myr timescales (Catuneanu *et al.*, 2000), it seems less likely that flexural tectonism in the Western Interior Foreland Basin has exerted a dominant control on fluvial aggradation or incision at 400 kyr timescales: the observed maximal duration and amplitude of incision of *ca* 200 kyr to create a *ca* 8 m deep valley corresponds to an erosion rate of 0.04 m kyr^{-1}. According to Catuneanu *et al.* (2000), the foredeep migrated at *ca* 10 m kyr^{-1} corresponding to 2 km migration in 200 kyr. This rate of foredeep migration is not likely to have caused the observed incisions.

Autogenic avulsion and allogenic climate control
Autogenic avulsions or channel migrations played an important role in the stratigraphic stacking within the clastic parts of the CCS, i.e. within the channel-splay dominated systems (Facies Association A, Table 1). Peat formation might have been autogenically controlled as well for specific intervals. For example, the lower U-coals do gradually pass into the lateral, muddy sediments of Facies B2. Here, peat compaction or channel infilling may have caused super-elevation, triggering muddy channel avulsions. On the larger scale (*ca* 10 km), the compaction of peat to coal in between the clastic units of the CCS is likely responsible for maintaining and accentuating a compensational stacking pattern. However, the observed lateral variability does not provide evidence that compensational stacking controlled the regional extent as well as the duration of peat formation (Facies C2), even though compensational stacking is an autogenic mechanism in itself (e.g. Hajek & Straub, 2017). the absence of syndepositional channel-belts of Facies A1 coeval with peat formation (Facies C2) suggests that alternations between these facies (CCS) are not formed by

autogenic avulsion. More specifically, an autogenic avulsion control on peat formation in fluvial systems would start with a syndepositional channel-belt system adjacent to backswamp peat formation; with time clastic-peat interfingering would be observed (e.g. McCabe, 1984). If the channel-belt becomes super-elevated with respect to the (compacting) peat, avulsion may be initiated (e.g. Fielding, 1984; Van Asselen *et al.*, 2009). The peat formation of Facies C2 which is decoupled from autogenic channel avulsions, possibly reflects regionally extensive peat mires. In absence of high sediment load, channels were poorly developed; possibly drainage was even diffusion-dominated (Whitfield *et al.*, 2009). The 100 kyr timescale involved with the recurrence of Facies C2 argues for a cyclic allogenic control. Similar to the underlying Tullock Member, the major peat-forming phases may originate from changes in the amount of sediment supply allogenically driven by short-eccentricity-paced climate changes (Noorbergen *et al.*, 2018).

Downstream base-level

The stratigraphic architecture of the three AIS (Fig. 7) resembles the sequence stratigraphic model of Wright & Marriott (1993). This model shows the maturity of soil development in relation to a geomorphic base-level control on fluvial aggradation and incision. Applied to the Lebo Shale Member, the aggradational part of the AIS, consisting of the successive CCS, would correspond to the high base-level/relative sea-level stages of Wright & Marriott (1993). Enhanced floodplain clastic sedimentation and weak soil development (conforming to Facies Association A) would be favoured if accommodation rates increased during base-level rise. In the subsequent highstand, reduced accommodation rates caused decreased clastic floodplain sedimentation, favouring increased soil development (conforming to Facies Association C). The incision part of the AIS representing the valley formation (lower part of Facies B1) and inter-valley soil-leaching (Facies B2) would then correspond to the low base-level stages of Wright & Marriott (1993). Namely, increased erosion creating fluvial valleys and coeval strong soil development on the terraces would be favoured if accommodation rates were low, during a low-stand. In the subsequent early-stage of base-level rise, slightly increased accommodation caused channel amalgamation and hydromorphic soil formation (upper part of Facies B1 and Facies B2).

The fluvial sequence stratigraphic model of Wright & Marriott (1993), however, is not universal, and several issues associated with this model have to be take into account. Firstly, base-level fall causing incision applies to settings where coastal plain gradients are significantly smaller than shelf gradients. If *vice versa*, base-level fall may lead to aggradation (e.g. Miall, 1991; Schumm, 1993; Holbrook, 1996; Blum & Törnqvist, 2000). Secondly, rivers can reorganize themselves in response to base-level changes by adapting their channel sinuosity and by modifying their channel geometries, especially in settings with small differences between coastal plain and shelf gradients (Lane, 1955; Schumm, 1993; Wescott, 1993; Holbrook, 1996; Wellner & Bartek, 2003; Swenson & Muto, 2007). Thirdly, the landward limit of base-level control on fluvial aggradation and incision varies with coastal plain gradients, ranging from *ca* 350 km for low-gradient, large river systems to *ca* 40 km for steep-gradient, small rivers (Blum & Törnqvist, 2000; Blum *et al.*, 2013).

Estimates of the longitudinal profile length and shape, and of the landward limit of sea-level effects are needed to tell whether base-level change could have been a driver of aggradation or incision in the Lebo Shale fluvial system. A reconstruction of the palaeo-environment would provide an estimation of the longitudinal profile gradient. A basin-scale examination of fossil flora preserved within the Palaeocene sediments of the Fort Union Formation indicates that this area was covered with lowland swamp vegetation extending for over *ca* 300 km, from the Cannonball Sea in the east to the foothills of the Rocky Mountains in the west (Brown, 1962). A basin-scale quantitative analysis of the megafloral record shows that vegetation was dominated by dicotyledonous angiosperm species, i.e. one major group of flowering plants, for 79% (Peppe, 2010). The brackish water tongues of the Cannonball Member, exposed along the Little Missouri River (Fig. 1B), are composed of dark black-brown mudstones that were likely deposited in lagoons during terrigenous inflow of clay and silt, derived from rivers draining a low-gradient coastal plain (Van Alstine, 1974). The overall fine grain sizes, brackish faunal associations (i.e. bivalves, crabs, ostracods and benthic foraminifera) and sedimentary facies associations (i.e. salt marsh, tidal flat, tidal channels, lagoon, mainland beaches, shoreface barriers and shelf) within the Slope and Cannonball Members have been linked

to the comparable coastal setting of the northern Netherlands (Cvancara, 1972, 1976; Fenner, 1974; Van Alstine, 1974). Nevertheless, Lindholm (1984) further specified that "*the Cannonball body of water*" in North-Dakota may have been one big lagoon, instead of a sea, and that different directions of sediment supply over the lagoon resulted in varying depositional environments and faunal compositions. Low continental shelf-gradients likely continued for several hundreds of kilometres, following a shallow inland continental seaway until open sea/ocean waters were reached in the south and/or in the north (Cvancara, 1986). There, at the Caribbean and/or Arctic shelf break, the gradient ultimately steepened along a continental slope.

A very low gradient profile is in agreement with channel slopes in the Lebo Shale Member ranging between 0.000026 and 0.000057 (Diemer & Belt, 1991). Given the up to *ca* 10 m thick sandstone bodies of Facies Association A (Table 1) and the minimal incision depths of 5.1 to 8.3 m for the fluvial valleys in the study area, the trunk channels crossing the study area can be assumed to have been less than 10 m deep. The lowest slope of 0.000026 (tangent) and the deepest trunk channel of 10 m (opposite) account for a maximum (adjacent) backwater length of 384.6 km, i.e. the inland distance at which sea-level change likely has an influence on the fluvial system (Blum *et al.*, 2013). Since the maximum transgressed shoreline of the Cannonball Sea was situated at *ca* 100 km distance from the study area (Fig. 1A), most – if not all – of the deposition of the Lebo Shale Member in the study area was in the backwater length. Nevertheless, without a significant difference between the low-angle coastal plain and the low-angle shelf gradients, it is not very likely that base-level change led to aggradation or incision to accommodate for longitudinal profile changes. Moreover, with a falling base-level causing headward incision, deep fluvial valleys and mature inter-valley soils would be expected to be present proximal to the coast, but such features have not been documented within the time-equivalent fluvial and deltaic strata of the Slope Member in downslope western Dakota (Belt *et al.*, 1984; Hartman, 1993; Warwick *et al.*, 2004; Peppe *et al.*, 2009). The rivers were probably able to reorganize themselves in response to base-level changes by adapting their channel sinuosity and/or by modifying their channel geometries (e.g. Lane, 1955; Miall, 1991; Schumm, 1993; Wescott, 1993; Holbrook, 1996;

Blum & Törnqvist, 2000; Wellner & Bartek, 2003; Swenson & Muto, 2007).

Global sea-level changes during long-eccentricity cycles

Looking specifically at eccentricity driven climate scenarios, 405 kyr cycles may have affected global (eustatic) sea-level changes in greenhouse worlds (Wendler *et al.*, 2014). Recent hydrological mass-balance calculations indicate that *ca* 30 m global sea-level changes in the mid-Cretaceous greenhouse world, with negligible glacio-eustasy, may result from orbital-paced changes in global groundwater storage, i.e. aquifer-eustasy (Wendler *et al.*, 2016). Eustatic sea-level fall would be in response to net storage of water in continental aquifers during an intensified hydrological cycle and enhanced fluvial run-off, while a relaxed hydrological cycle causes aquifer discharge exceeding aquifer charge inducing eustatic sea-level rise (Sames *et al.*, 2016; Wendler & Wendler, 2016). This scenario envisages eustatic sea-level lowstands during 405 kyr long-eccentricity maxima as a consequence of an intensified hydrological cycle during eccentricity modulated high-amplitude precession forcing and eustatic sea-level highstands during 405 kyr long-eccentricity minima as a consequence of a relaxed hydrological cycle during low-amplitude precession-forcing. The aquifer-eustatic sea-level would be falling during transitions from long-eccentricity minima to maxima and rising vice versa.

Upstream climate

A plausible alternative for downstream base-level rise is that regional climate changes occurred upstream and were paced by long-eccentricity control on the AIS formation in the Lebo Shale Member. Upstream regional climate, predominantly through the effect of precipitation and temperature changes, exerts a significant influence on fluvial environments by its control on vegetation, weathering, erosion, discharge and sediment supply (e.g. Knox, 1972; Summerfield, 1991; Vandenberghe, 2003). Several studies have shown how river channels adjusted their patterns and styles in response to different changes in hydrological regimes related to Quaternary climate change (e.g. Schumm, 1968a; Baker, 1977; Baker & Penteado-Orellana, 1977; Bogaart & Van Balen, 2000; Bridgland, 2000; Goodbred, 2003; Tandon *et al.*, 2006; Roy *et al.*, 2012; Blum *et al.*, 2013; Vandenberghe, 2015). Baker & Penteado-Orellana (1977) studied

the response of the Colorado River in central Texas (USA) to late Quaternary climate change and suggested that incision is triggered by enhanced occurrence of rare high-magnitude flooding events in an arid glacial climate. Nevertheless, such a fluvial response to arid climate contradicts with the Palaeocene–Eocene Thermal Maximum (PETM) of the Bighorn Basin (USA), where an arid climate regime is responsible for fluvial sheet-sandstone aggradation instead of incision (Foreman, 2014). The observation that the valley-related facies of AIS-2 occur towards or during a stable climate without major extremes, i.e. long eccentricity minima (Fig. S2), a process other than high-magnitude peak discharges in an arid climate might have caused the incision. Given the three to four 100 kyr CCS prevailing between the valley-fills of the three AIS, the AIS-1 and AIS-3 incisions do likely share the same phase relation with long-eccentricity as the AIS-2 incision.

Unfortunately, it remains elusive at this stage whether the fluvial incisions started towards or within long-eccentricity minima due to resolution constraints in the age model. Nonetheless, the prolonged reduction of the precession-amplitude associated with long-eccentricity minima could have resulted in a relaxation of the hydrological cycle over approximately 200 kyr long intervals. The presence of higher frequency precession-induced climate variations that occur superimposed on this stable background climate may have determined the onset of incision. Fluvial incision could only have been triggered if discharge significantly exceeded sediment supply (e.g. Blum & Törnqvist, 2000), although both absolute amounts of discharge and sediment supply are expected to diminish in a climate with less extremes at times of the long-eccentricity minima (i.e. low amplitude precession cycles). A constant supply of moisture from the Pacific in the west and/or from the Cannonball Sea in the east to the source areas of the drainage network might have promoted the development of a dense vegetation cover upstream. This upstream vegetation reduces erosion and thus sediment supply to the drainage system (e.g. Schumm, 1968b). On the other hand, discharge might have remained stable, especially if it would not be significantly reduced by high evapotranspiration (Bogaart & Van Balen, 2000). Enhanced moisture supply in particular might have caused peak discharge events that cannot be buffered by evapotranspiration. Thus, towards and/or within the long-eccentricity minima, the AIS incisions in the Lebo Shale Member might have been triggered during short intensifications of the hydrological cycle within the longer-term stable climate interval.

The impact of vegetation on fluvial incision during global sea-level rise agrees well with the fluvial terraces in north-western Europe that were created by river incision during Late Glacial global sea-level rise (Bridgland, 2000; Vandenberghe, 2015) and has been confirmed by numerical modelling (Bogaart & Van Balen, 2000). In this case fluvial incision is indirectly linked to the upstream development of vegetation, with relatively low evapotranspiration, causing a strong reduction in sediment supply with respect to discharge.

The sediments eroded by the AIS incisions in the Lebo Shale Member would have been deposited downstream, especially when entering the low-energy flow regime of the Cannonball lagoon (Lindholm, 1984). This downstream sediment deposition may have resulted in local delta progradation overruling the aquifer-eustatic sea-level rise component (Wendler & Wendler, 2016). It might thus be that long-eccentricity upstream climate control on fluvial incision causes local-scale progradation and, hence, locally an opposite sea-level motion, i.e. lowering fall rather than a rise predicted by aquifer-eustasy.

The termination of fluvial incision could have taken place when at a certain valley-floor depth the equilibrium fluvial graded profile was reached at which discharge and sediment supply were in balance. As an alternative for or in addition to the lowering valley floor, the continuing aquifer-eustatic sea-level rise during the long-eccentricity minima could also have caused the termination of incision and likely enabled the switch to aggradation. Namely, the backwater-induced rising floodwater level of the river enables inundation of the valleys which causes a marked reduction of the stream power in the river channel. As a consequence, enhanced sediment supply over discharge stopped incision and enabled the constitution of the fine sediment load bayou system responsible for the mud-prone valley-infill aggradation.

Conceptual stratigraphic model

Figure 8 shows stratigraphic architectural models, depicting an AIS formed over one 405 kyr long-eccentricity cycle. Concerning the formation of a CCS, the current model adopts the short-eccentricity-scale model of Noorbergen *et al.* (2018, option 2).

In consideration of long-eccentricity climate control, it should be noted that the influence of eccentricity alone on climate is very small. Nevertheless long-eccentricity climate control is significant because eccentricity modulates the amplitude of the precession cycle and hence the seasonal contrast (e.g. Hilgen *et al.*, 2015). The highest seasonal contrasts in the Northern Hemisphere occur in high amplitude precession minima during eccentricity maxima (highest ellipsoidal orbit). Northern Hemisphere's lowest seasonal contrast takes place in high amplitude precession maxima during eccentricity maxima. Constantly low seasonal contrasts do occur during low amplitude precession cycles during eccentricity minima. Because of the important role of precession on climate, precession is included in the model (Fig. 8).

Stage I – Peat aggradation

Relatively low amplitude precession cycles in the early stages of the transition from a long-eccentricity minimum to maximum are providing conditions for a relatively stable climate without major seasonal extremes. During the relaxed hydrological cycle, a constant moisture supply to the drainage network causes low erosion and high evapotranspiration. As a consequence, both sediment supply and discharge are low. A high aquifer-eustatic sea-level provides suitable wetland conditions for widespread peat formation across densely vegetated mires.

Stage II – Clastic aggradation

High amplitude precession cycles during a long-eccentricity maximum result in an unstable climate with major seasonal extremes during the precession minima. These stages cause an intensified hydrological cycle. Enhanced seasonal precipitation and droughts during the precession minima cause distinct hinterland erosion. The resultant sediment supply along the graded profile significantly exceeds discharge which leads to clastic aggradation. During wet season(s) sediments are distributed by splays and laterally migrating channels while during dry season(s) lowered groundwater-levels induce sediment oxidation on the overbanks. Peat accumulation is prevented as overbank vegetation is frequently overwhelmed by the sediment floods. Besides fluvial aggradation the high sediment supply causes deltaic progradation. In combination with an aquifer-eustatic sea-level lowstand sea-level further regresses resulting in a base-level drop.

Stage III – Incision and inter-valley soil formation

Lowered amplitude precession cycles towards or within a long-eccentricity minimum causes climate to stabilize because of a reduction in seasonal contrasts. This causes relaxation of the global hydrological cycle. Aquifer-eustatic sea-level rise results in base-level rise. Long-term constant moisture supply to the hinterland source areas cause an expanding vegetation cover upstream with increasing, but still relatively low, evapotranspiration. Sediment supply reduces due to upstream reduction of erosion by the vegetation cover and is now in deficit with respect to discharge. The channel incises and creates a valley. Repeated incisions during high discharge events, particularly during the higher seasonality precession minima, confine the stream flow along the valleys. Groundwater levels lower towards the valley bottom and leached soil profiles develop on the inter-valley platforms. The eroded sediments are deposited coastward as a consequence of reduced energy conditions downstream. As a result, this sediment supply may locally overrule aquifer-eustatic sea-level rise causing progradation at those locations.

Stage IV – Channel stabilization and incipient peat formation

Low amplitude precession cycles during a long-eccentricity minimum constitute for a stable climate without major seasonal extremes. This causes a relaxed global hydrological cycle. The vegetation cover upstream is at its maximum extent causing very low sediment supply downstream. Discharge exceeds sediment supply at times of reduced evapotranspiration, mostly during slightly enhanced seasonality in the low-amplitude precession minima. At the same time, base-level rises to its maximum point during an aquifer-eustatic sea-level highstand. The backwater effects of the marine transgression cause high river floodwater levels upstream. The valleys inundate and the stream power of the river channel reduces, promoting aggradation when particularly muddy sediments are sporadically supplied. When the indurated inter-valley soils are inundated there is energy dispersal over the extensive platforms which give rise to the development of a low-energy muddy bayou system. The stable wet climate conditions cause high organic production and the accumulation of these organics produces peat bodies (Stage V, equivalent to Stage I).

CONCLUSIONS

Age control and time-stratigraphic correlations in a *ca* 15 km long stratigraphic fence panel of the fluvial Lebo Shale Member in north-eastern Montana reveal the presence of ten 100 kyr scale coal–clastic successions (CCS) and three 400 kyr scale aggradation–incision sequences (AIS). Magnetostratigraphic correlation shows that polarity chron C28r, with a duration of 224 kyr (Dinarès-Turell *et al.*, 2014), spans the upper part of AIS-2 and lower part of AIS-3 (Fig. 7). This implies that the second fluvial incision phase, i.e. the incision of AIS-2, corresponds to the transition from long-eccentricity maximum to minimum or to the minimum itself (Fig. S2). Separated by three to four short-eccentricity-scale CCS (Noorbergen *et al.*, 2018), the AIS-1 and AIS-3 incisions seem to occur during the same long-eccentricity configurations.

The origin of the AIS follows from a critical evaluation of possible tectonic, base-level and upstream climate control on their formation. Foreland basin flexural tectonism, and associated cyclic creation of positive or negative space for sedimentation, acted on *ca* 5 Myr timescales in the Western Interior Basin between the Campanian and Palaeocene. An estimate made on the rate of foredeep migration appeared not likely to have caused the observed incisions. At times of deposition, coastal plain gradients were likely higher than shelf gradients making it unlikely that base-level fall triggered headward fluvial incision. It is also not very likely that base-level change led to aggradation or incision to accommodate for longitudinal profile changes along the low-angle coastal plain and shelf gradients. Rivers were probably able to reorganize themselves in response to base-level induced profile changes by adapting their channel sinuosity and/or by modifying their channel geometries. Furthermore, no valley and inter-valley soils are documented in time-equivalent deltaic deposits in North-Dakota which would have been expected if base-level fall had caused headward fluvial incision. Fluvial aggradation and incision were likely in response to long-eccentricity-forced upstream changes in sediment supply and discharge. In the stable climate background of long-eccentricity minima, fluvial incision could have been repeatedly triggered when discharge was enhanced relative to sediment supply when the latter was being reduced by an expanding vegetation cover upstream. The incision may have sustained until a fluvial equilibrium was autogenically established and/or the

stream power was reduced because the valley floor inundated enabled by backwater-induced floodwater level rise of the river. Continued base-level rise and reduced stream power possibly caused aggradation of mostly fine-grained sediments. The deposition of the fine-grained sediment load in a meandering bayou would then have produced the low-angle inclined mud-rich palaeovalley-fills of the Lebo Shale Member. The model of Fig. 8 provides a reference for recognizing fluvial aggradation–incision sequences regulated by long-eccentricity forcing.

CONFLICT OF INTEREST

The authors do not have any conflict of interest.

DATA AVAILABILITY STATEMENT

The data that supports the findings of this study are available in the supplementary material of this article.

REFERENCES

Abels, H.A., **Kraus, M.J.** and **Gingerich, P.D.** (2013) Precession-scale cyclicity in the fluvial lower Eocene Willwood Formation of the Bighorn Basin, Wyoming (USA). *Sedimentology*, **60**, 1467–1483.

Baker, V.R. (1977) Adjustment of fluvial systems to climate and source terrain in tropical and subtropical environments. *Fluv. Sedimentol. Mem.*, **5**, 211–230.

Baker, V.R. and **Penteado-Orellana, M.M.** (1977) Adjustment to Quaternary climatic change by the Colorado River in central Texas. *J. Geol.*, **85**, 395–422.

Beaumont, C. (1981) Foreland basins. *Geophys. J. Int.*, **65**, 291–329.

Belt, E. (1993) Tectonically induced clastic sediment diversion and the origin of thick, widespread coal beds (Appalachian and Williston basins, USA). In: *Tectonic Controls and Signatures in Sedimentary Successions* (Ed. Belt, E.S.), pp. 377–397. John Wiley & Sons, Hoboken.

Belt, E.S., Flores, R.M., Warwick, P.D., Conway, K.M., Johnson, K.R. and Waskowitz, R.S. (1984) Relationship of fluviodeltaic facies to coal deposition in the Lower Fort Union Formation (Paleocene), South-Western North Dakota. In: *Sedimentology of Coal and Coal-bearing Sequences* (Eds Caraher, W. and Conway, K.), pp. 177–195. John Wiley & Sons, Hoboken.

Belt, E.S., Hartman, J.H., Diemer, J.A., Kroeger, T.J., Tibert, N.E. and Curran, H.A. (2004) Unconformities and age relationships, Tongue River and older members of the Fort Union Formation (Paleocene), western Williston Basin, USA. *Rocky Mountain Geol.*, 39, 113–140.

Blum, M.D. and Törnqvist, T.E. (2000) Fluvial responses to climate and sea-level change: a review and look forward. *Sedimentology*, 47, 2–48.

Blum, M., Martin, J., Milliken, K. and Garvin, M. (2013) Paleovalley systems: insights from Quaternary analogs and experiments. *Earth Sci. Rev.*, 116, 128–169.

Bogaart, P.W. and Van Balen, R.T. (2000) Numerical modeling of the response of alluvial rivers to Quaternary climate change. *Global Planet. Change*, 27, 147–163.

Bohor, B.F. and Triplehorn, D.M. (1993) Tonsteins: altered volcanic ash layers in coal-bearing sequences. *Geol. Soc. Am.*, 285, 1–44.

Bridgland, D. (2000) River terrace systems in north-west Europe: an archive of environmental change, uplift and early human occupation. *Quatern. Sci. Rev.*, 19, 1293–1303.

Brown, R.W. (1962) Paleocene flora of the Rocky Mountains and great Plains. *Geol. Surv. Prof. Pap.*, 375, 1–263.

Burns, C., Mountney, N., Hodgson, D. and Colombera, L. (2017) Anatomy and dimensions of fluvial crevasse-splay deposits: examples from the Cretaceous Castlegate Sandstone and Neslen Formation, Utah, USA. *Sed. Geol.*, 351, 21–35.

Catuneanu, O. (2006) *Principles of Sequence Stratigraphy*. Elsevier, Amsterdam, pp. 1–375.

Catuneanu, O., Beaumont, C. and Waschbusch, P. (1997) Interplay of static loads and subduction dynamics in foreland basins: reciprocal stratigraphies and the "missing" peripheral bulge. *Geology*, 25, 1087–1090.

Catuneanu, O., Sweet, A. and Miall, A. (2000) Reciprocal stratigraphy of the Campanian-Paleocene western interior of North America. *Sed. Geol.*, 134, 235–255.

Chadima, M. and Hrouda, F. (2006) Remasoft 3.0 a user-friendly paleomagnetic data browser and analyzer. *Trav. Géophys.*, 27, 20–21.

Cherven, V.B. and Jacob, A.F. (1985) Evolution of Paleogene depositional systems, Williston Basin, in response to global sea level changes. In: *Cenozoic Paleogeography of the West-Central United States*, Rocky Mountain Section (SEPM), 127–170.

Clyde, W.C., Ramezani, J., Johnson, K.R., Bowring, S.A. and Jones, M.M. (2016) Direct high-precision U-Pb geochronology of the end-Cretaceous extinction and calibration of Paleocene astronomical timescales. *Earth Planet. Sci. Lett.*, 452, 272–280.

Collier, A.J. and Knechtel, M.M. (1939) The coal resources of McCone county. *US Geol. Surv. Bull.*, 905, 80. US Government Printing Office, Montana.

Cvancara, A. (1972) Summary of the Cannonball Formation (Paleocene) in North Dakota. *North Dakota Geological Survey Miscellaneous Series*, 50, 69–75.

Cvancara, A.M. (1976) Geology of the Cannonball Formation (Paleocene) in the Williston Basin, with reference to uranium potential. *North Dakota Geological Survey Report of investigation*, 57 (No. GJO–1633-3), 1–22. Department of Geology, University of North Dakota.

Cvancara, A.M. (1986) The Cannonball Formation (Paleocene) of central-most North America. *North Dakota Geological Society 2008 – Tertiary and Upper Cretaceous of South-Central and Western North Dakota: 1986 Field Trip*, 23–24.

DeCelles, P.G. (2004) Late Jurassic to Eocene evolution of the Cordilleran thrust belt and foreland basin system, western USA. *Am. J. Sci.*, 304, 105–168.

Diemer, J.A. and Belt, E.S. (1991) Sedimentology and paleohydraulics of the meandering river systems of the Fort Union Formation, southeastern Montana. *Sed. Geol.*, 75, 85–108.

Dinarès-Turell, J., Westerhold, T., Pujalte, V., Röhl, U. and Kroon, D. (2014) Astronomical calibration of the Danian stage (Early Paleocene) revisited: settling chronologies of sedimentary records across the Atlantic and Pacific Oceans. *Earth Planet. Sci. Lett.*, 405, 119–131.

Durkin, P.R., Hubbard, S.M., Boyd, R.L. and Leckie, D.A. (2015) Stratigraphic expression of intra-point-bar erosion and rotation. *J. Sed. Res.*, 85, 1238–1257.

Eberth, D.A. (1996) Origin and significance of mud-filled incised valleys (Upper Cretaceous) in southern Alberta, Canada. *Sedimentology*, 43, 459–477.

Ethridge, F.G., Wood, L.J. and Schumm, S. (1998) Cyclic variables controlling fluvial sequence development: problems and perspectives. *SEPM Spec. Publ.*, 59, 17–29.

Fastovsky, D.E. and Bercovici, A. (2016) The Hell Creek Formation and its contribution to the Cretaceous-Paleogene extinction: a short primer. *Cretac. Res.*, 57, 368–390.

Fenner, W.E. (1974) The foraminiferids of the Cannonball Formation (Paleocene, Danian) and their paleoenvironmental significance: Grant, Morton and Oliver Counties, North Dakota. Doctoral dissertation, University of North Dakota, 1–135.

Fielding, C. (1984) A coal depositional model for the Durham Coal Measures of NE England. *J. Geol. Soc.*, 141, 919–931.

Fielding, C.R. and Webb, J.A. (1996) Facies and cyclicity of the Late Permian Bainmedart coal measures in the Northern Prince Charles Mountains, MacRobertson Land, Antarctica. *Sedimentology*, 43, 295–322.

Fisher, R. (1953) Dispersion on a sphere. *Proc. Roy. Soc. London A Math. Phys. Eng. Sci.*, 217, 295–305.

Flores, R.M. (2003) Paleocene paleogeographic, paleotectonic, and paleoclimatic patterns of the northern Rocky Mountains and Great Plains region. In: *Cenozoic Systems of the Rocky Mountain Region*, Rocky Mountain Section (SEPM), 63–106.

Flores, R. and Keighin, C. (1999) Fort Union coal in the Williston Basin, North Dakota: a synthesis. *US Geol. Surv. Prof. Pap. A*, 1625, 1–45.

Flores, R., Keighin, C., Ochs, A., Warwick, P., Bader, L. and Murphy, E. (1999) Framework geology of Fort Union coal in the Williston Basin. *Fort Union Assessment Team, US Geol. Surv. Prof. Pap.*, 1625-A, 1–64.

Foreman, B. (2014) Climate-driven generation of a fluvial sheet sand body at the Paleocene-Eocene boundary in northwest Wyoming (USA). *Basin Res.*, 26, 225–241.

Gibling, M.R. (2006) Width and thickness of fluvial channel bodies and valley fills in the geological record: a literature compilation and classification. *J. Sed. Res.*, 76, 731–770.

Goodbred, S.L., Jr (2003) Response of the Ganges dispersal system to climate change: a source-to-sink view since the last interstade. *Sed. Geol.*, 162, 83–104.

Guccione, M., **Burford, M.** and **Kendall, D.** (1999) Pemiscot Bayou, a large distributary of the Mississippi River and a possible failed avulsion. *Fluvial Sedimentology VI. Special Publication of the International Association of Sedimentologists*, **28**, 211–220.

Hajek, E.A. and **Straub, K.M.** (2017) Autogenic sedimentation in clastic stratigraphy. *Annu. Rev. Earth Planet. Sci.*, **45**, 681–709.

Hartman, J.H. (1993) Road log to the type areas of the Paleocene Slope Formation and intercalated tongues of the Cannonball Formation, Slope County, North Dakota. *North Dakota Geological Society 2008 – The Marshall Lambert Symposium*, 78–86.

Hilgen, F.J., **Hinnov, L.A.**, **Aziz, H.A.**, **Abels, H.A.**, **Batenburg, S.**, **Bosmans, J.H.**, **de Boer, B.**, **Hüsing, S.K.**, **Kuiper, K.F.**, **Lourens, L.J.** and **Rivera, T.** (2015) Stratigraphic continuity and fragmentary sedimentation: the success of cyclostratigraphy as part of integrated stratigraphy. *Geol. Soc. London Spec. Publ.*, **404**, 157–197.

Holbrook, J.M. (1996) Complex fluvial response to low gradients at maximum regression; a genetic link between smooth sequence-boundary morphology and architecture of overlying sheet sandstone. *J. Sed. Res.*, **66**, 713–722.

Holbrook, J. and **Schumm, S.A.** (1999) Geomorphic and sedimentary response of rivers to tectonic deformation: a brief review and critique of a tool for recognizing subtle epeirogenic deformation in modern and ancient settings. *Tectonophysics*, **305**, 287–306.

Holbrook, J., **Scott, R.W.** and **Oboh-Ikuenobe, F.E.** (2006) Base-level buffers and buttresses: a model for upstream versus downstream control on fluvial geometry and architecture within sequences. *J. Sed. Res.*, **76**, 162–174.

Holdgate, G., **Wallace, M.**, **O'Connor, M.**, **Korasidis, V.** and **Lieven, U.** (2016) The origin of lithotype cycles in Oligo-Miocene brown coals from Australia and Germany. *Int. J. Coal Geol.*, **166**, 47–61.

Johnson, K.R., **Nichols, D.J.** and **Hartman, J.H.** (2002) Hell Creek Formation: a 2001 synthesis. *Geol. Soc. Am. Spec. Pap.*, **361**, 503–510.

Kirschvink, J. (1980) The least-squares line and plane and the analysis of palaeomagnetic data. *Geophys. J. Int.*, **62**, 699–718.

Knox, J.C. (1972) Valley alluviation in southwestern Wisconsin. *Ann. Assoc. Am. Geogr.*, **62**, 401–410.

Korasidis, V.A., **Wallace, M.W.**, **Wagstaff, B.E.**, **Holdgate, G.R.**, **Tosolini, A.P.** and **Jansen, B.** (2016) Cyclic floral succession and fire in a Cenozoic wetland/peatland system. *Palaeogeogr. Palaeoclimatol. Palaeoecol.*, **461**, 237–252.

Koymans, M.R., **Langereis, C.G.**, **Pastor-Galán, D.** and **van Hinsbergen, D.J.** (2016) Paleomagnetism.org: an online multi-platform open source environment for paleomagnetic data analysis. *Comput. Geosci.*, **93**, 127–137.

Kraus, M.J. (1999) Paleosols in clastic sedimentary rocks: their geologic applications. *Earth Sci. Rev.*, **47**, 41–70.

Lane, E.W. (1955) Importance of fluvial morphology in hydraulic engineering. *Proc. Am. Soc. Civ. Eng.*, **81**(paper no.745), 1–15.

Laskar, J., **Robutel, P.**, **Joutel, F.**, **Gastineau, M.**, **Correia, A.** and **Levrard, B.** (2004) A long-term numerical solution for the insolation quantities of the Earth. *Astron. Astrophys.*, **428**, 261–285.

LeCain, R., **Clyde, W.C.**, **Wilson, G.P.** and **Riedel, J.** (2014) Magnetostratigraphy of the Hell Creek and lower fort union formations in northeastern Montana. *Geol. Soc. Am. Spec. Pap.*, **503**, 137–147.

Leopold, L.B. and **Bull, W.B.** (1979) Base level, aggradation, and grade. *Proc. Am. Philos. Soc.*, **123**, 168–202.

Lindholm, R.M. (1984) Bivalve associations of the Cannonball Formation (Paleocene, Danian) of North Dakota. Master thesis, University of North Dakota, 1–75.

Mackin, J.H. (1948) Concept of the graded river. *Geol. Soc. Am. Bull.*, **59**, 463–512.

Martinsen, O.J., **Ryseth, A.L.F.**, **Helland-Hansen, W.**, **Flesche, H.**, **Torkildsen, G.** and **Idil, S.** (1999) Stratigraphic base level and fluvial architecture: Ericson sandstone (Campanian), rock springs uplift, SW Wyoming, USA. *Sedimentology*, **46**, 235–263.

McCabe, P.J. (1984) Depositional environments of coal and coal-bearing strata. In: *Sedimentology of Coal and Coal-bearing Sequences* (Eds Rahmani, R.A. and Flores, R.M.), pp. 11–42. John Wiley & Sons, Hoboken.

McCarthy, P.J. and **Plint, A.G.** (1999) Floodplain palaeosols of the Cenomanian Dunvegan Formation, Alberta and British Columbia, Canada: micromorphology, pedogenic processes and palaeoenvironmental implications. *Geol. Soc. London Spec. Publ.*, **163**, 289–310.

McCarthy, P.J. and **Plint, A.G.** (2003) Spatial variability of palaeosols across Cretaceous interfluves in the Dunvegan Formation, NE British Columbia, Canada: palaeohydrological, palaeogeomorphological and stratigraphic implications. *Sedimentology*, **50**, 1187–1220.

Miall, A.D. (1985) Architectural-element analysis: a new method of facies analysis applied to fluvial deposits. *Earth Sci. Rev.*, **22**, 261–308.

Miall, A.D. (1991) Stratigraphic sequences and their chronostratigraphic correlation. *J. Sed. Res.*, **61**, 497–505.

Miall, A.D. (2014) *Fluvial Depositional Systems*. Springer, Berlin, pp. 1–316.

Noorbergen, L.J., **Abels, H.A.**, **Hilgen, F.J.**, **Robson, B.E.**, **de Jong, E.**, **Dekkers, M.J.**, **Krijgsman, W.**, **Smit, J.**, **Collinson, M.E.** and **Kuiper, K.F.** (2018) Conceptual models for short-eccentricity-scale climate control on peat formation in a lower Paleocene fluvial system, north-eastern Montana (USA). *Sedimentology*, **65**, 775–808.

Ogg, J. (2012) Geomagnetic polarity time scale. In: *The Geologic Time Scale* (Eds Gradstein, F.M., Ogg, J.G., Schmitz, M.D. and Ogg, G.M.), pp. 85–113. Elsevier, Amsterdam.

Olsen, H. (1990) Astronomical forcing of meandering river behaviour: Milankovitch cycles in Devonian of East Greenland. *Palaeogeogr. Palaeoclimatol. Palaeoecol.*, **79**, 99–115.

Olsen, H., **de, Boer, P.** and **Smith, D.** (1994) Orbital forcing on continental depositional systems – lacustrine and fluvial cyclicity in the Devonian of East Greenland. In: *Orbital Forcing and Cyclic Sequences*. International Association of Sedimentologists, Special Publication, 429–438.

Peppe, D.J. (2010) Megafloral change in the early and middle Paleocene in the Williston Basin, North Dakota, USA. *Palaeogeogr. Palaeoclimatol. Palaeoecol.*, **298**, 224–234.

Peppe, D., **Evans, D.** and **Smirnov, A.** (2009) Magnetostratigraphy of the Ludlow Member of the Fort Union Formation (Lower Paleocene) in the Williston Basin, North Dakota. *Geol. Soc. Am. Bull.*, **121**, 65–79.

Posamentier, H. and **Vail, P.** (1988) Eustatic controls on clastic deposition II—sequence and systems tract models. *SEPM Spec. Publ.*, **42**, 125–154.

Potter, J., **PetroGraphics, J.**, **McIlreath, I.** and **Natras, T.** (2008) Lithotypes, Macerals and coal facies studies of Lower Cretaceous Medicine River Coals in South Central Alberta: applications in CBM exploration, depositional environments and tectonic history studies. In: *Back to Exploration*. pp. 777–780. AAPG Geoconvention 2008, Calgary.

Rigby, J. and **Rigby, J., Jr** (1990) Geology of the Sand Arroyo and Bug Creek Quadrangles, McCone County, Montana. *Brigham Young Univ. Geol. Stud.*, **36**, 69–134.

Roy, N., **Sinha, R.** and **Gibling, M.** (2012) Aggradation, incision and interfluve flooding in the Ganga Valley over the past 100,000 years: testing the influence of monsoonal precipitation. *Palaeogeogr. Palaeoclimatol. Palaeoecol.*, **356**, 38–53.

Sames, B., **Wagreich, M.**, **Wendler, J.**, **Haq, B.**, **Conrad, C.**, **Melinte-Dobrinescu, M.**, **Hu, X.**, **Wendler, I.**, **Wolfgring, E.** and **Yilmaz, I.** (2016) Short-term sea-level changes in a greenhouse world—a view from the Cretaceous. *Palaeogeogr. Palaeoclimatol. Palaeoecol.*, **441**, 393–411.

Schumm, S.A. (1968a) River adjustment to altered hydrologic regimen, Murrumbidgee River and paleochannels, Australia. *US Geol. Surv. Prof. Pap.*, **598**, 1–63. US Government Printing Office.

Schumm, S. (1968b) Speculations concerning paleohydrologic controls of terrestrial sedimentation. *Geol. Soc. Am. Bull.*, **79**, 1573–1588.

Schumm, S. (1993) River response to baselevel change: implications for sequence stratigraphy. *J. Geol.*, **101**, 279–294.

Shanley, K.W. and **McCabe, P.J.** (1994) Perspectives on the sequence stratigraphy of continental strata. *AAPG Bull.*, **78**, 544–568.

Smith, N.D. and **Pérez-Arlucea, M.** (2004) Effects of peat on the shapes of alluvial channels: examples from the Cumberland Marshes, Saskatchewan, Canada. *Geomorphology*, **61**, 323–335.

Sprain, C.J., **Renne, P.R.**, **Wilson, G.P.** and **Clemens, W.A.** (2015) High-resolution chronostratigraphy of the terrestrial Cretaceous-Paleogene transition and recovery interval in the Hell Creek region, Montana. *Geol. Soc. Am. Bull.*, **127**, 393–409.

Sprain, C.J., **Feinberg, J.M.**, **Renne, P.R.** and **Jackson, M.** (2016) Importance of titanohematite in detrital remanent magnetizations of strata spanning the Cretaceous-Paleogene boundary, Hell Creek region, Montana. *Geochem. Geophys. Geosyst.*, **17**, 660–678.

Sprain, C.J., **Renne, P.R.**, **Clemens, W.A.** and **Wilson, G.P.** (2018) Calibration of chron C29r: new high-precision geochronologic and paleomagnetic constraints from the Hell Creek region, Montana. *Geol. Soc. Am. Bull.*, **130**, 1615–1644.

Stone, R.W. and **Calvert, W.R.** (1910) Stratigraphic relations of the Livingston Formation of Montana. *Econ. Geol.*, **5**, 551–557.

Straub, K.M., **Paola, C.**, **Mohrig, D.**, **Wolinsky, M.A.** and **George, T.** (2009) Compensational stacking of channelized sedimentary deposits. *J. Sed. Res.*, **79**, 673–688.

Summerfield, A. (1991) *Global Geomorphology*. Longman, Harlow, pp. 1–547.

Swenson, J.B. and **Muto, T.** (2007) Response of coastal plain rivers to falling relative sea-level: allogenic controls on the aggradational phase. *Sedimentology*, **54**, 207–221.

Swisher, C.C., III, **Dingus, L.** and **Butler, R.F.** (1993) 40Ar/39Ar dating and magnetostratigraphic correlation of the terrestrial Cretaceous-Paleogene boundary and Puercan

Mammal Age, Hell Creek-Tullock formations, eastern Montana. *Can. J. Earth Sci.*, **30**, 1981–1996.

Tandon, S., **Gibling, M.**, **Sinha, R.**, **Singh, V.**, **Ghazanfari, P.**, **Dasgupta, A.**, **Jain, M.** and **Jain, V.** (2006) Alluvial valleys of the Ganga Plains, India: timing and causes of incision. *SEPM Spec. Publ.*, **85**, 15–35.

Thébault, E., **Finlay, C.C.**, **Beggan, C.D.**, **Alken, P.**, **Aubert, J.**, **Barrois, O.**, **Bertrand, F.**, **Bondar, T.**, **Boness, A.**, **Brocco, L.** and **Canet, E.** (2015) International geomagnetic reference field: the 12th generation. *Earth, Planets and Space*, **67**, 79.

Triplehorn, D.M., **Stanton, R.W.**, **Ruppert, L.F.** and **Crowley, S.S.** (1991) Volcanic ash dispersed in the Wyodak-Anderson coal bed, Powder River basin, Wyoming. *Org. Geochem.*, **17**, 567–575.

Van Alstine, J.B. (1974) Paleontology of brackish-water faunas in two tongues of the Cannonball Formation (Paleocene, Danian), Slope and Golden Valley Counties, southwestern North Dakota. Doctoral dissertation, University of North Dakota, 1–92.

Van Asselen, S., **Stouthamer, E.** and **Van Asch, T.W.** (2009) Effects of peat compaction on delta evolution: a review on processes, responses, measuring and modeling. *Earth Sci. Rev.*, **92**, 35–51.

Vandenberghe, J. (2003) Climate forcing of fluvial system development: an evolution of ideas. *Quatern. Sci. Rev.*, **22**, 2053–2060.

Vandenberghe, J. (2015) River terraces as a response to climatic forcing: formation processes, sedimentary characteristics and sites for human occupation. *Quatern. Int.*, **370**, 3–11.

Vandenberghe, N., **Hilgen, F.J.** and **Speijer, R.** (2012) The paleogene period. In: *The Geologic Time Scale 2012* (Eds Gradstein, F.M., Ogg, J.G., Schmitz, M. and Ogg, G.), pp. 855–921. Elsevier, Amsterdam.

Warwick, P.D., **Flores, R.M.**, **Nichols, D.J.** and **Murphy, E.C.** (2004) Chronostratigraphic and depositional sequences of the Fort Union Formation (Paleocene), Williston Basin, North Dakota, South Dakota, and Montana. In: *Sequence Stratigraphy, Paleoclimate, and Tectonics of Coal-bearing Strata: AAPG Studies in Geology* (Eds Pashin, J.C. and Gastaldo, R.A.), 51st edn, 121–125. American Association of Petroleum Geologists (AAPG), Tulsa.

Wellner, R.W. and **Bartek, L.R.** (2003) The effect of sea level, climate, and shelf physiography on the development of incised-valley complexes: a modern example from the East China Sea. *J. Sed. Res.*, **73**, 926–940.

Wendler, J.E. and **Wendler, I.** (2016) What drove sea-level fluctuations during the mid-Cretaceous greenhouse climate? *Palaeogeogr. Palaeoclimatol. Palaeoecol.*, **441**, 412–419.

Wendler, J.E., **Meyers, S.R.**, **Wendler, I.** and **Kuss, J.** (2014) A million-year-scale astronomical control on Late Cretaceous sea-level. *Newsl. Stratigr.*, **47**, 1–19.

Wendler, J.E., **Wendler, I.**, **Vogt, C.** and **Kuss, J.** (2016) Link between cyclic eustatic sea-level change and continental weathering: evidence for aquifer-eustasy in the Cretaceous. *Palaeogeogr. Palaeoclimatol. Palaeoecol.*, **441**, 430–437.

Wescott, W.A. (1993) Geomorphic thresholds and complex response of fluvial systems–some implications for sequence stratigraphy. *AAPG Bull.*, **77**, 1208–1218.

Whitfield, P.H., **St-Hilaire, A.** and **van der Kamp, G.** (2009) Improving hydrological predictions in peatlands. *Can. Water Resour. J.*, **34**, 467–478.

Woolsey, L.H., **Richards, R.W.** and **Lupton, C.T.** (1917) The bull mountain coal field. *US Geol. Surv. Bull.*, **647**, 218. Musselshell and Yellowstone Counties, Montana. US Government Printing Office.

Wright, V.P. and **Marriott, S.B.** (1993) The sequence stratigraphy of fluvial depositional systems: the role of floodplain sediment storage. *Sed. Geol.*, **86**, 203–210.

Supporting Information

Additional information may be found in the online version of this article:

Figure S1. Zijderveld diagrams of thermal (TH) and alternating field (AF) demagnetization of characteristic samples underpinning the magnetostratigraphy of the Lebo Shale Member in the study area.

Figure S2. Relation between short-eccentricity and long-eccentricity in polarity chron C28r in marine sections (Zumaia, site 1262, site 1209) is linked to the aggradation–incision sequences in the Lebo Shale.

Table S1. Magnetostratigraphic data of thermally demagnetized samples.

Table S2. Magnetostratigraphic data of samples demagnetized with alternating fields.

Data S1. Data-file-1_Noorbergen_Palaeomagnetism_Thermal.th

Data S2. Data-file-2_Noorbergen_Palaeomagnetism_Alternating-field.AF

Appendix S1. Demagnetization results